

Article

Not peer-reviewed version

The Particularity of the Warm Rain in Catalonia

[Francesc Figuerola](#)*, [Dolors Ballart](#), [Tomeu Rigo](#), [Montse Aran](#)

Posted Date: 10 March 2026

doi: 10.20944/preprints202510.0233.v2

Keywords: warm rain; forecast; Catalonia; thermodynamics; floods; remote sensing



Preprints.org is a free multidisciplinary platform providing preprint service that is dedicated to making early versions of research outputs permanently available and citable. Preprints posted at Preprints.org appear in Web of Science, Crossref, Google Scholar, Scilit, Europe PMC.

Copyright: This open access article is published under a [Creative Commons CC BY 4.0 license](#), which permit the free download, distribution, and reuse, provided that the author and preprint are cited in any reuse.

Disclaimer/Publisher's Note: The statements, opinions, and data contained in all publications are solely those of the individual author(s) and contributor(s) and not of MDPI and/or the editor(s). MDPI and/or the editor(s) disclaim responsibility for any injury to people or property resulting from any ideas, methods, instructions, or products referred to in the content.

Article

The Particularity of the Warm Rain in Catalonia

Francesc Figuerola *, Dolors Ballart, Tomeu Rigo and Montse Aran

Area de Predicció i Vigilància, Servei Meteorològic de Catalunya, Dr. Roux, 80, 08013, Barcelona, Spain

* Correspondence: francesc.figueroles@gencat.cat

Abstract

Warm rain events occur when moist air masses containing elevated precipitable water produce high rainfall rates capable of generating local flash floods. Catalonia, located on the northeastern Mediterranean coast of the Iberian Peninsula, is regularly affected by such episodes: approximately 70% of daily precipitation events exceeding 10 mm with fewer than ten cloud-to-ground lightning flashes can be classified as warm rain. The current research aimed to identify the meteorological conditions most conducive to heavy warm rain episodes in Catalonia. These cases are commonly associated with flash flood episodes in the study region. We have utilized rain gauges, lightning data, radar, and model fields, combined with radio sounding profiles. First, we have identified and characterized warm rain cases, and secondly, we have selected some relevant cases to characterize the phenomenon. These events occur predominantly along the Catalan coast during the warm season, typically following the passage of a cold front, and are associated with shallow convective clouds producing little or no lightning. However, the key determining factor is a characteristic vertical thermodynamic profile: a moist and saturated lower troposphere with high precipitable water beneath a low- to mid-level thermal inversion, weak instability concentrated near the surface. Furthermore, local wind convergence plays a principal role in the rainfall pattern.

Keywords: warm rain; forecast; Catalonia; thermodynamics; floods; remote sensing

1. Introduction

Warm rain is defined as precipitation generated in a cloud with temperatures at all levels exceeding 0 °C [1–5]. Therefore, warm rain-producing clouds are characterized by the absence of ice phase inside [6,7]. The predominant process of drop formation is coalescence, that is, the merging by collision of two water drops into a single larger drop [2,8]. Warm rain occurs in clouds that have sufficient liquid water content, upward flow, and duration to sustain the process of growing by coalescence, which generates size drops of drizzle or rain [2,9]. Furthermore, Nelson (1971) [10] demonstrated that a zone of higher liquid content facilitates the coalescence process, which produces rainfall in a reasonable time. In fact, this type of rainfall-producing mechanism generates a rapid conversion of water vapor to rain, resulting in high precipitation efficiency and rainfall rates [11].

This type of precipitation plays a major role in the global water cycle [2]. Similarly, Beard and Ochs (1993) [4] found that most of the rain produced in the tropics is associated with clouds entirely warmer than freezing. The analysis by Ohtake (1963) [12] of 62 radiosonde stations, distributed between the tropical regions and high latitudes (Alaska), observed that warm rain is more frequent than expected. He observed that the precipitating regime was very different, with a seasonal pattern in the medium and high latitudes (summer events). Meanwhile, warm rain events are common throughout the year in the tropical region. Besides the warm rain, there exists another type of precipitation with similar characteristics: supercooled warm rain (associated with aircraft icing [9]). In this case, the precipitation can reach a temperature of –5 °C or less without changing to ice crystals [13]. For this type of rainfall, the relative humidity must verify the same conditions as those of the classical warm rain.

From the point of view of the upper-air sounding data [12], the factors to be accomplished in warm rain events are a layer with relative humidity exceeding 80% under the iso-zero level, while the mass air just above this level must be 20% drier than ice saturation at any temperature. The first point means that warm clouds have formed below the 0 °C level, meanwhile the second one implies that ice crystals do not exist over iso-zero. Another analysis made using radiosonde data was presented by [9]. That study considered a database of 25 years with nearly 1000 radiosondes covering the full United States area, except the Rocky Mountain States. The first discrimination was done considering the cloud-top temperature (CTT), the presence of a warm layer (WL), and the relative position of both, CTT and WL. It was concluded that the warm rain process was responsible for the freezing precipitation in 47% of the soundings in which this type of precipitation was observed. [14] analyzed the meteorological conditions observed in events that affected the south-facing slopes of the Hawaiian Islands. Values of thermodynamics for the soundings before the events indicated scarce instability (only KI showed values associated with strong instability), while one of the key features was the moisture rise between 750 and 450 hPa. This last characteristic was highly correlated with the events of high precipitation amounts. The large amount of humidity at medium levels plays a major role in the events because of two factors: firstly, the entrainment of air with a higher virtual temperature into the rising parcel, and, on the other hand, the suppression of the formation of a cold downdraft.

Ref. [15] analyzed data from a nine-year period of the Tropical Rainfall Measuring Mission (TRMM) from a global point of view of the areas more affected by warm rain. They found that the systems of small vertical depth have been considered the main contributors to the total precipitation in those areas where recorded values are minimum. More specifically, [16] used the same data for the analysis of warm rain in the Tropics. Their work was since warm rain over tropical oceans could be produced by stratocumuli or by well-developed cumuli. The main results obtained in the study were that precipitation echoes with cloud-top temperatures exceeding 0 °C contributed to 20% of the total rainfall over tropical oceans and 7.5% over tropical land. It is important to note that about 50% of the pixels over the ocean and two-thirds of the pixels over land are associated with cold precipitation systems. Furthermore, large amounts of warm rain occur during winter over oceans near windward coasts. Mesoscale warm rain systems with strong radar echoes occur in all areas of the tropical oceans, mainly at night rather than during daytime [16]. The mean heights of warm rain over the ocean are lower than over land. Finally, they didn't observe significant regional variability in the sizes and intensities of warm rain in the tropics. Another study based on TRMM data (Lau and Wu, 2003) [7] showed that warm rain accounted was 31% of the total rain amount, being 72% of the total rain area in the tropical areas. In the same work, the Authors proved that the precipitation production per unit for cloud liquid water increases as Sea Surface Temperature (SST) rises, in the case of weak warm rain. From this last result, they concluded that more warm rain cases will be squeezed out from the low and mid-levels of the cloud, in a future warmer climate. In the same way, Kodama et al. (2009) [3] showed that in the tropics, subtropics, and part of the mid-latitudes, the warm rain accumulation over the ocean had a positive correlation with the SST; however, the dependency of SST on total rain was exclusive of the tropics. On the other hand, [17] also considered satellite data to analyze the dependence of timescale formation processes in warm rain events.

The high sea surface temperature of the Mediterranean Sea compared to the surface temperature over land is one of the most important factors that help the development of storms [18]. [19] have shown that most events affecting the Mediterranean Basin were produced mainly between August and October. However, it is also important that all the months of the year register at least 5 cases during the century. In any case, in this work, it was not distinguished between deep convective and warm rain events.

Refs. [20,21] presented some different features observed in episodes of warm rain in the Mediterranean region. Firstly, weak wind is observed at mid and high levels and low vertical shear. The fact that cold air masses exist at high levels implies that the cloud top reaches high altitudes and that the Convective Available Potential Energy (CAPE) value is high. At the same time, the cloud

base is placed at a very low altitude while the instability is relatively high, considering that the layer in which the instability is observed is moderately narrow. Furthermore, we can summarize from these works other important features of warm rain events: first, the elevated rain rate during short time periods [22]; deep convection rarely occurs; and low lightning activity [5,21,23]. In contrast to the case of warm rain, most heavy rain events in the Mediterranean area are associated with Deep Convection (see some examples in [24,25]). This type of event is characterized by high vertical development of the clouds and the coexistence of liquid and solid phases. This combination can result in huge amounts of rainfall during short time periods. Furthermore, it is associated with an important lightning activity [26,27]. In terms of Surveillance tasks, one of the most complicated aspects is the coexistence of cold convective precipitation and warm rain in the same event. Therefore, regions with different precipitation characteristics can remain quite close in time and space. For example, this fact was previously documented in the region in at least one previous case (October 1994), in which remote sensing tools didn't identify the presence of warm, efficient rain [28].

Warm rain events are caused by small vertical and horizontal shallow cumulus convection [23]. Their small size [29] implies that remote sensing tools usually don't warn of their intensity. Furthermore, a larger part of the cloud extends below the freezing level or just over the thermal inversion level [30]. Therefore, these clouds can't develop deeply, and they appear in infrared (IR) satellite images as low and warm clouds [16,29,31], instead of the typical white and organized bright top deep convection clouds. On the other hand, the lack or low presence of ice phase in this cloudiness is the reason for few if any cloud-to-ground lightning [32,33]. And finally, reflectivity radar values show moderate to high reflectivity but always concentrated at the lower part of the cloud [12,29,32–34]. On the other hand, meteorological models don't seem to predict these events with accuracy because the thermodynamic environment only shows low instability [35–37]. Consequently, they become an issue to the population, but also a threat and a challenge for forecasters.

One of the regions where warm rain has been extensively studied is Hawaii [22,38,39]. [22] analyzed the rainfall rate of Hawaiian showers. They found unexpectedly high rainfall rates over brief intervals of time, with intensity peaks exceeding 100 mm/h and rates of 150 mm/h. The trade wind inversion, normally present at an altitude of about 2 km, usually prevents the vertical development of updrafts necessary for the formation of thunderstorms [38]. They found that subtropical high-pressure cells cause almost constant strong trade wind inversions that limit the vertical development of most clouds. Consequently, clouds were all warm, and their tops were situated below 3,5 km. Despite their small dimensions, sharp bursts of relatively high-intensity rainfall of brief duration occurred frequently, which suggested relatively high Precipitable Water Content (PWC). However, practically no rainfall occurred if the inversion base was less than 2 km high. Moreover, 68 percent warm rain showers associated with the trade winds during September and October 1973 occurred during nighttime. Finally, [39] reached similar conclusions: cloud depth, which determines the showers' initiation, was estimated primarily by the inversion height. The strong inversion was around 2 km, with high humidity below this height.

On the other hand, two decades before, [40] found similar characteristics of Hawaiian warm-cloud rainfall events in Puerto Rico warm rain: the trade inversion, well established in winter, limited cloud development, with cloud tops confined between 2400 m and 3500 m ASL; consequently, warm clouds grew well below the freezing level, that was situated from 4300 to 4600 m ASL.

Based on the previous information, the RLR (Rainfall-Lightning-Ratio) parameter should present high values in cases of warm rain events. The RLR is estimated using the rate between cumulated rainfall and the cloud-to-ground sum over a particular area [41,42]. In most of the previous analyses, RLR is estimated based on quantitatively estimated precipitation from weather radar and lightning flashes. However, in our case, we have used rainfall from rain gauges to consider a longer data series. Bearing in mind that deep convective rainfall events (with a very high number of flashes) have low RLR values, we have searched for the opposite: high RLR values, because of the null or scarce contribution of lightning activity.

The warm rain episodes studied here normally occur in a peculiar interaction between the Global Atmospheric Circulation (GAC), the SST, and the orography of Catalonia and nearby areas [43,44]. During the year, and due to the GAC, the weather is governed by the flow of polar depressions that bring cold air masses from northern latitudes. When these low-pressure systems reach the study area, they encounter several mountain ranges that modify the wind flow. Consequently, this fact implies hindering the intrusion of the cold air. These ranges include the Pyrenees, the Iberian System, the Massif Central, and the Alps.

As shown in Figure 1, the northerly and northwesterly winds, upon reaching the Iberian Peninsula and the North-Western Mediterranean Basin, are forced to channel through the Ebro Valley, the Rhône Valley, and the Aquitaine Region due to the presence of the Pyrenees, the Iberian System, the Massif Central, and the Alps. When these fourth-quadrant winds cross Catalonia, they displace the pre-existing air mass—warmer and more humid—and introduce a new one that is colder and drier. However, this process does not affect the entire territory. The central sector of the coastal and pre-coastal areas remains sheltered at low levels from these general north-westerly winds due to the influence of the major mountain ranges mentioned above, as well as smaller ranges within Catalonia itself. Consequently, in this area, the warm and humid Mediterranean air tends to persist for some days. On the other hand, northerly and north-westerly flow generates a mesoscale low on the leeward side of the Pyrenees. This low produces a return flow that advects the warm maritime air that remains sheltered toward this part of the coast and partially the inland regions of Catalonia. It is in this small pocket of warm, moist Mediterranean maritime air where warm rain develops. In addition, this warm and humid air mass often generates an arc of clouds, sometimes narrow and sometimes wide, that receives the name of “Estela Pirinenca” (“Pyrenean Wake”) [44].

For this reason, most events studied have occurred after a cold front crossing Catalonia. Only in a few cases, warm rain events have been observed in another synoptic framework that, though, maintains the same maritime air mass. In consequence, these kinds of heavy rain, as in other places in the world [33,39,45], are directly related to maritime air and SST, which provide a huge quantity of humidity. The higher the SST is, the higher the supply of PWM from the sea is [46]. This fact occurs mainly during summer and autumn. So, it is in these two seasons that the most intense events occur.

A particularity of the Pyrenean Wake is the interplay of forces between the two winds that arrive at Catalonia: the northern wind that arrives from the Gulf of Lion and the eastern edge of the Pyrenees range, called “Tramuntana”, and the northwestern one that arrives at Catalonia from the Ebro Valley, called “Mestral”. If Tramuntana is stronger than Mestral, the Pyrenean Wake will develop in the central and southern parts of the Catalan coast. If Mestral is stronger than Tramuntana, the arc of clouds and convergence zone will form at the central and northern parts of the coast. And finally, if they have the same strength, the arm of cloudiness will develop on the central coast.

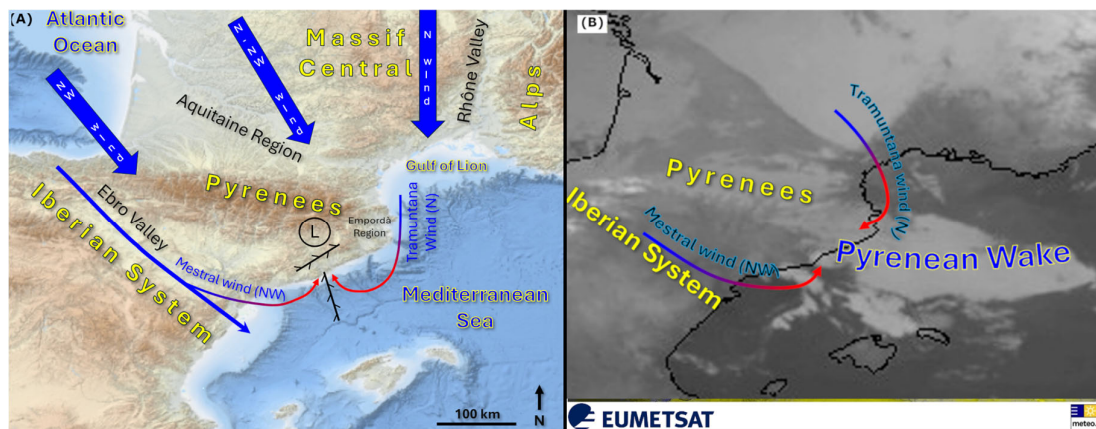


Figure 1. (A) Orographic map of the west Mediterranean Sea basin and southwest of Europe, showing the main sea and ocean, mountain ranges, valleys and regions. Wide blue arrows are northerly and north-westerly

synoptic flow/wind. Thin blue-to-red arrows are canalized winds (cold and dry at their origin -in blue- and warm and moist at their end after travelling over the Mediterranean Sea -in red-). "L" is the leeward mesoscale low. The black thin line with small bowed black lines at each side indicates a convergence line. (B) Infrared image from the Meteosat 11 satellite, for 16 July 2020 at 02:00 UTC, during case B of heavy warm rain from Table 2. The Pyrenean Wake goes from inland Catalonia up to Mediterranean Sea.

The purpose of our research is to introduce the heavy warm rain episodes occurring in Catalonia. The first part of the analysis consists of identifying warm rain events in Catalonia for the period 2006-2025, based on the RLR parameter using rain gauges and cloud-to-ground flashes. Once we have characterized the events from a point of view of time and space, we have identified some meteorological characteristics of the events through (mesoscale and synoptic) model fields, thermodynamic soundings, and radar and satellite images. This knowledge should serve as a preliminary database of cases and, on the other hand, improve the forecasting and surveillance tools of these events that cause adverse issues to the Catalan population.

2. Area of Study and Data Used

2.1. The Area of Interest

The Area of Interest includes all the Catalan territory (Figure 2), located in the northeastern part of the Iberian Peninsula. The region is characterized by a complex topography, with mountains reaching 3000 m in the Pyrenees (running from west to east in the northern part of the area), and the 1700 m and 700 m in the Prelitoral and Litoral Ranges, respectively (both going discontinuously from southwest to northeast, nearly parallel to the coast). Therefore, the valleys and mountains are relevant factor in most events, because the complex orography allows the formation of local wind convergences. In any case, the maritime nature of the air mass that generates this rainfall means that most of the episodes occur in the shaded blue area in Figure 2 (panel b). This area is known as the combination of the Litoral and Prelitoral sectors.

Going deeper with the region of interest (the Central Litoral and Prelitoral), it is modeled by the two previously cited chains: the Prelitoral and Litoral ranges. These two chains set a very steep terrain, full of small basins of streams. Due to their short length and the mountain slopes, these streams are characterized by a fast-time hydrological response, making them prone to flash floods. Furthermore, this region is the most populated zone of Catalonia, with more than 6,8 million inhabitants [47]. Therefore, the combination of all factors (heavy rainfall, complex hydrology, and highly vulnerable territory) can turn the small but intense warm rain events into a hazard for the population.

2.2. Data Used

The period of study was from 2006, when the EPV realized the importance of these events, until 30 November 2025 (a total of 7274 days). The analyzed events have been chosen according to the parameter presented more extensively in Section 3.1 (RLR), which can be summarized as the relationship between the rainfall provided by rain gauges and cloud-to-ground flashes detected close to each rainfall measurement point (within a distance closer than 5 km). The following subsections present the different types of data used to analyze the selected events. #

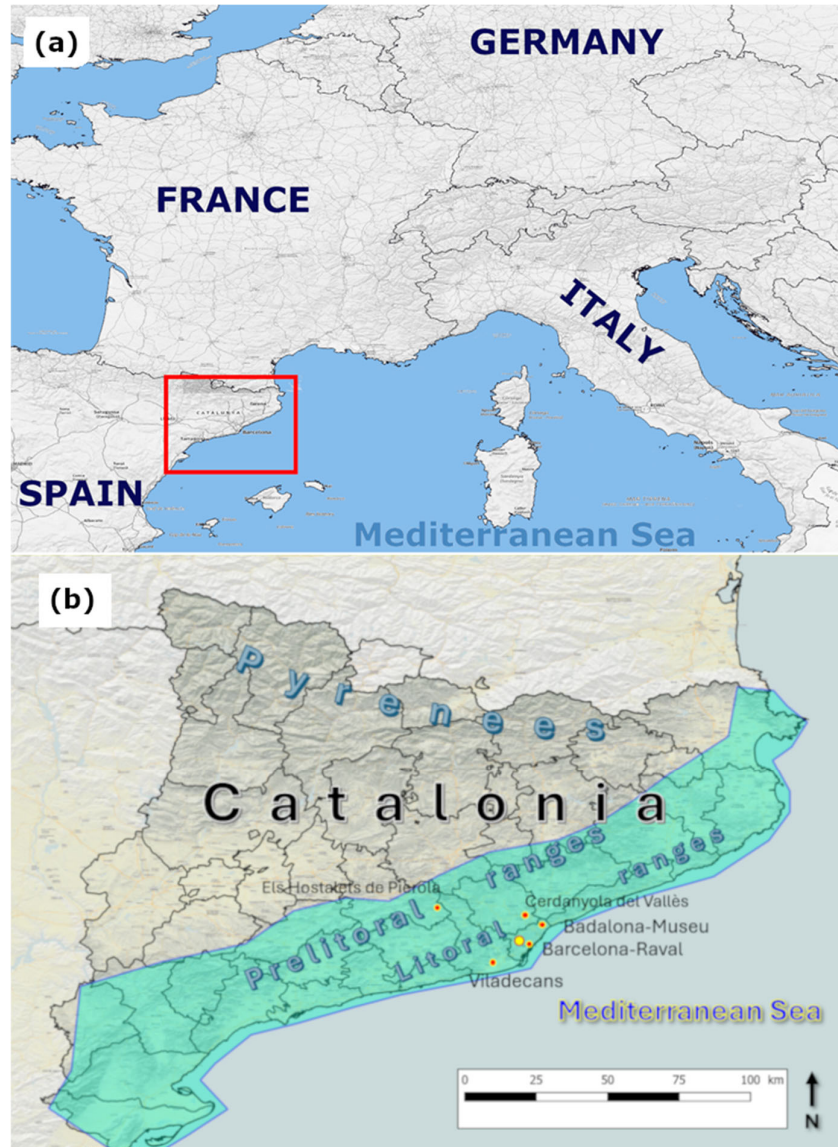


Figure 2. (a) Map of the western Mediterranean Sea basin. The red rectangle indicates the area of interest (zoomed on the bottom panel). (b) Political and orographic map of Catalonia. The red dots show the location of the warm rain events presented in Table 2. The yellow dot is the atmospheric sounding station of Barcelona (code 08190 of WMO). This cyan-shaded polygon indicates the region usually affected by warm rain events.

2.2.1. Surface Observations

The Automatic Weather Stations Network (or XEMA, from the Catalan “Xarxa d’Estacions Meteorològiques Automàtiques”) is managed by the SMC. It is composed of 190 Stations (see Figure 3), which transmit information to the SMC quarters via digital radio, GSM (Global System for Mobile communications) technology, and satellite. The main variables provided are rainfall at 1-minute time resolution, and wind (direction and speed), humidity, temperature, and solar radiation at 30-minute time resolution [48]. Despite the high density, there are several cases in which none of the stations can report high rainfall values. This is because of the small area with precipitation. In the current analysis, we have used the 24-hour cumulated data to select those days with precipitation exceeding the 10 mm threshold (this allows reducing the total number of candidate days). After this, we have considered 1-hour rainfall to estimate the RLR for each day.

2.2.2. Upper-Air Observations

The atmospheric Barcelona sounding station has been operative since 1998 and has the World Meteorological Organization (WMO) code 08190 [49]. It allows us to know the vertical profile of the atmosphere on the central coast twice a day (0 and 12 UTC). The study has focused on the CAPE values [50] and vertical distribution, the precipitable water mass content (PWM) and distribution along the vertical profile [7], and the equilibrium level (EL), freezing level (FRZG), and Lifted Condensation Level (LCL) heights [7,51]. CIN (or Convection Inhibition) [52,53] is also provided in the sounding profiles, but it has not been specifically analyzed in the current Research. These variables can provide relevant information to determine the main relevant features and, furthermore, to identify a common pattern that can help to a better forecast of these events.

2.2.3. Remote Sensing

Three types of remote sensing data have been used. Integrating all sources is possible for the development of a full scheme of warm rain clouds. The high quality in time and space of all systems plays a major role in the analysis of the event, especially for surveillance tasks. The sources are:

- The SMC radar network (XRAD) is composed of four Doppler single-pol radars [54]. Each of them operates on C-band and has a maximum range of 250 km, with only one elevation or Plan Position Indicator (PPI) field at this range. Furthermore, the short-range provides volumetric information from 16 elevations, from 0.6 to 30°. The XRAD has been designed to provide quantitative rainfall estimates and 3D information on the rainfall-producing structures. The different products used in this analysis are reflectivity fields, or CAPPI (Constant Altitude Plan Position Indicators) at different heights; TOP12 (or the maximum height at which the 12 dBZ reflectivity threshold has been observed); and the precipitation estimation. Several types of external factors affect the quality of the radar imagery. In the case of the XRAD, they can be summarized as: on one hand, producing reflectivity overestimation (ground clutter, non-meteorological atmospheric echoes, and electromagnetic interferences) and, on the other hand, producing reflectivity underestimation (beam topographic blockage, radar beam elevation with distance, the cone of silence, and high-reflectivity blockage). These anomalies can interfere with the radar fields from different viewpoints [55]. La Miranda radar (LMI label in Figure 3) was installed in 2008; meanwhile, the others were put in operation between 2001 and 2003. Radar products have been used to characterize the precipitation regime on the specific events analyzed.
- The Lightning Detection Network (known as XDDE) has four VHF (Very High Frequency) plus LF (Low Frequency) interferometer detectors, which send individual data from each flash [56]. The complete information of every lightning strike is processed in a system in the SMC headquarters. The arrangement of the detectors was designed to provide good coverage for all of Catalonia, with precision in pinpointing lightning of 500 meters throughout a large part of the Catalan territory. Radar parameters have been compared with flash counts (cloud-to-ground, CG, and intra-cloud, IC). Amposta sensor (AMP label in Figure 3) was installed in 2006. The other sensors started their operational task between 2002 and 2004. The CG data from XDDE has been used mainly in the identification of events based on the RLR parameter estimation (see section 3.1)
- Satellite imagery proceeds from the Meteosat Second Generation (MSG) [57]. The MSG has three channels in the thermal infrared (7, 9, and 10). They allow the measurement of surface and cloud temperature. In the present study, only channel 9 has been used, and it corresponds to the thermal infrared. This channel monitors cloud dynamics throughout the day. The study of the imagery in the present work has been exclusively qualitative for the different selected episodes.

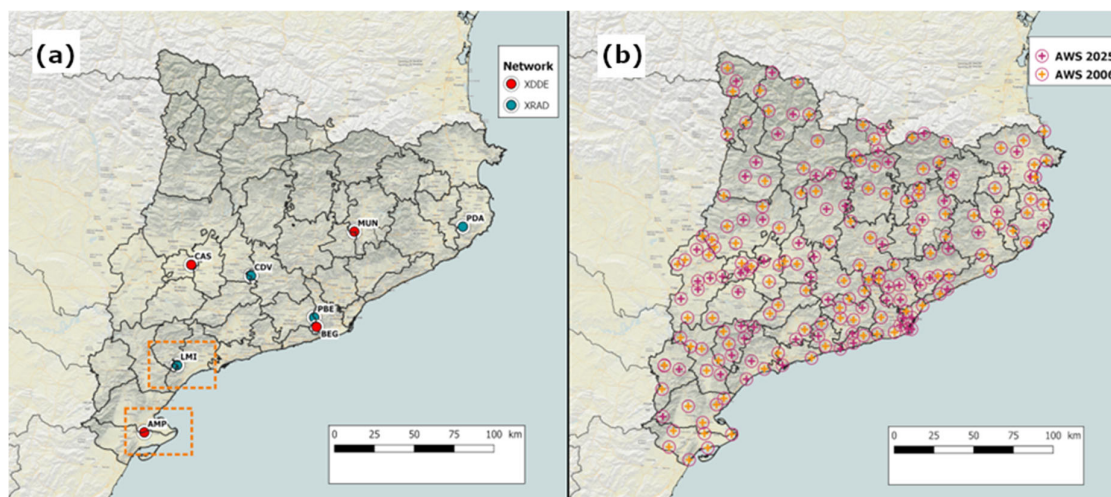


Figure 3. (a) Location of the sensors of the main SMC remote sensing networks used in the present study: Radar Network (XRAD), in blue, and the Lightning Detection Network (XDDE), in red. (b) Position of the Automatic Weather Stations network (XEMA) in 2006 (orange circles) and added since then, updated to 2025 (purple circles).

2.2.4. Numerical Weather Prediction (NWP) Models

Warm rain forecasting is based on two NWP configurations (Table 1): on one hand, synoptical (or large-scale), and, on the other hand, mesoscale (or mid-scale). The large-scale model used in this Research has been the European Centre for Medium-Range Weather Forecasts (ECMWF) [58,59]; meanwhile, the mesoscale operational model is Weather Research and Forecasting (WRF) [60].

The surface, 850 hPa, 500 hPa, and 300 hPa fields were analyzed for the large scale to identify the favorable atmospheric environment for warm rain events. The general pattern in those cases was behind a cold front or behind an upper-level trough. On the other hand, mesoscale outputs were used to obtain meteorological features at lower spatial resolution. In particular, these features were convergence lines, combined with signatures at low-level moisture fields. These elements helped to trigger convective clouds. #

Table 1. Scheme of the synoptic and mesoscale models used in the Research.

Model	Scale	Configuration
ECMWF (European Center Median Weather Forecasting)	Synoptic	0.5/0.25° grid, 3 hours, 60 levels, 144 hours horizon
WRF	Mesoscale	3/1.5 km grid, 3/1 hour, 31 levels, 72/48 hours horizon

The Research has considered two types of NWP (Numerical Weather Prediction) models to study and forecast the meteorological conditions of convective rainfall events, both warm and cold: large-scale and mesoscale. The first ones provide a global view of the atmospheric configuration from many days in advance. However, the large-scale models only provide some information about the occurrence feasibility of these events at large threats. The reason is the complexity of the object of study and the small size of the rain-producing clouds. Mesoscale models give us a better understanding of the evolving conditions in which warm rain events occur in Catalonia. Besides, the improvement of these models in recent years, combined with increasing experience, has helped to a better understanding of the outputs. In any case, the main limitation of the mesoscale models is the inability to forecast more than three days in advance of the event. Besides, the complex conditions during those events imply that the output does not always fit the reality. However, mesoscale models give indications to the forecasters at the time of warning the population. Furthermore, recent versions of NWP models sometimes provide rainfall forecast outputs with overestimated values, which lead

to false alarms. The different models and fields used in the past or currently are briefly presented in the following paragraphs.

3. Methodology

3.1. RLR

[32] studied the occurrence of warm rain events in Catalonia, considering radar fields (Quantitative Precipitation Estimation, QPE) and lightning data, searching for events with more than 10 mm/day with less than ten cloud-to-ground flashes per event. This analysis showed that most cases (73%) in the region for the period 2015-2022 verified both conditions. Rain Lightning Ratio (RLR) is an indicator of thunderstorm activity in heavy rain events [61–63]. Considering that warm rain events present situations with high rainfall values and low cloud-to-ground flashes, this parameter should have larger values in these episodes.

To identify possible candidates for warm rain events, we applied a technique similar to [32] but estimating rainfall from automatic rain gauges of the SMC network rather than radar fields. This provides more precise rainfall values, though the data are point measurements rather than a 2D field. We selected events with daily rainfall exceeding 10 mm and estimated the relationship between rainfall and lightning activity by considering the total number of cloud-to-ground flashes detected the same day within 5 km of the rain gauge. RLR was calculated as the ratio between rainfall measured by the gauge and the number of nearby flashes during a day.

Considering that warm rain events produce effective precipitation and few or null cloud-to-ground flashes, as shown in the introduction, we have selected those days with daily rainfall in some AWS exceeding 10 mm and CG under the threshold of ten. In consequence, we have removed those days with maximum precipitation below 10 mm or with more than 10 CG flashes. This preliminary selection allows 5,500 days to be discarded from the initial number of days (7,274, between 1 January 2006 and 30 November 2025), which corresponds to 72% of the total number of cases. In consequence, the first selection includes 2,133 candidate days. Another option to do the selection is to consider an RLR threshold. Considering the values of this ratio compared with the precipitation and CG values (see Figure 4), we have evaluated two options: 5 and 10 (mm per flash). The first one provides a list of 3,653 days, whereas the second one reduces the number of cases to 2,650. However, both selections (using CG and accumulation or using RLR) are limited due to the brief nature of the events (usually less than one hour) compared to the length of the source data (daily precipitation and lightning registers). Therefore, they should be refined considering hourly precipitation.

Figure 5 presents the process scheme considered in the Research, from the initial data (QPE and CG) for the day's selection with potential warm rain occurrence, to the meteorological analysis and the generation of a conceptual model.

We have evaluated several properties of events (hourly, monthly, and yearly evolutions, as well as spatial distribution). This has allowed us to get a preliminary characterization of the warm rain events in Catalonia. From here, we have selected a set of events to determine the principal meteorological properties of this type of precipitation in Catalonia, based on weather radar, AWS, NWP models, and radio-soundings.

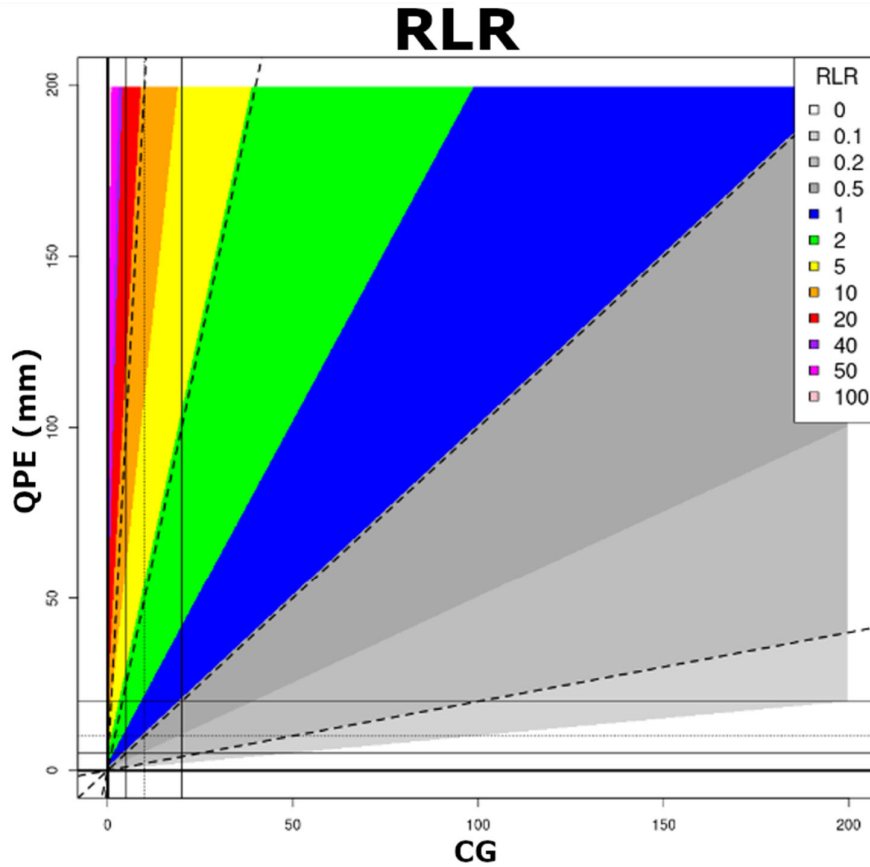


Figure 4. The RLR (Rainfall Lightning Rate) scheme for the different lightning (CG, x-axis) and rainfall (QPE, y-axis) values.

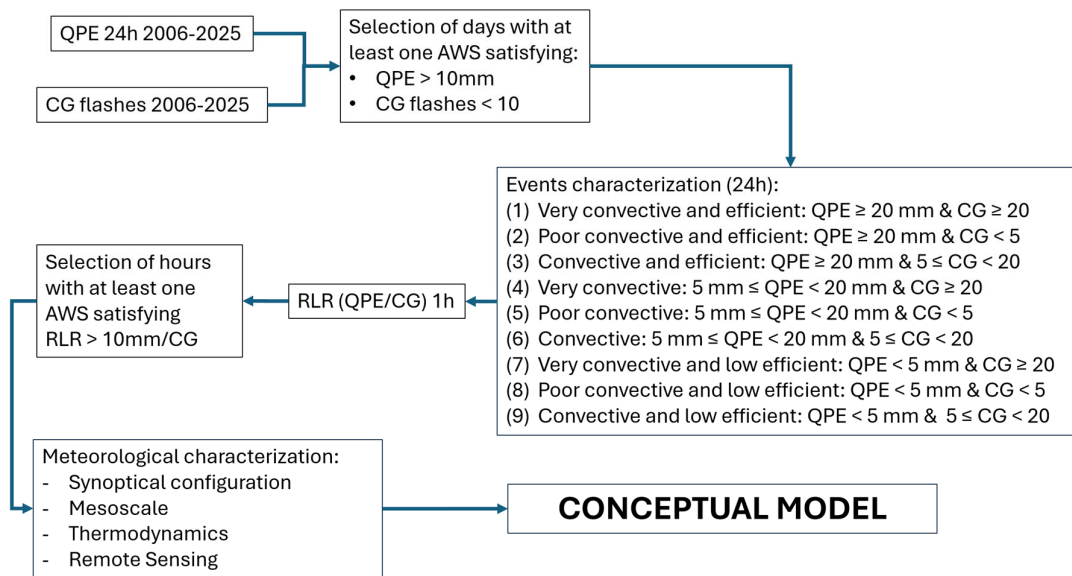


Figure 5. Conceptual scheme of the methodology used in the present Research for the selection of the events, the classification, and the final development of a conceptual model.

3.2. Contextualization of the Selected Events

We have selected four representative cases to illustrate the characteristics of the warm rain events in Catalonia, from different viewpoints, based on the tools previously presented. The different signatures observed in all cases help us to develop the conceptual model of this kind of event in the region of study. Concretely, the selected events were 2 September 2019, 16 July 2020, 18 December 2020, and 15 October 2023. The usual period for warm rain events in Catalonia is July to October. However, we have selected one case out of this season. This case demonstrates that the necessary conditions can occur even on dates outside the favorable season.

The selection has been made considering events that occurred after the passing of a trough or a cold front. Furthermore, the Pyrenean Wake pattern was well formed, and local wind convergences occurred in all cases. In addition, we have selected two cases that occurred in the coastal zone and two more in the pre-coastal area. Furthermore, three of the cases recorded heavy rainfall rates (higher than 30 mm in 30 minutes), and one case recorded huge amounts of precipitation (over 250 mm in only 12 hours).

4. Results

4.1. The Behavior of RLR Along the Period

Figure 6 shows the distribution of events (days) according to the relationship between lightning (CG flashes per day) and cumulated daily rainfall. There has been a predominance of Type 8 (poor convective and low efficiency cases, 91.17%), followed by Type 5 (poor convective, 5.67%) and Type 2 (poor convective but efficient, 1.62%) events. On the contrary, only 1.18% of cases were convective (between 5 and 20 CG), and 0.36% of days were very convective (more than 20 CG). In consequence, possible warm rain events (associated with Type 2) are more probable than the full set of convective and very convective days. Since this point, we will focus exclusively on days when candidates registered warm rain in at least one rain gauge (1,763 of the 7,724).

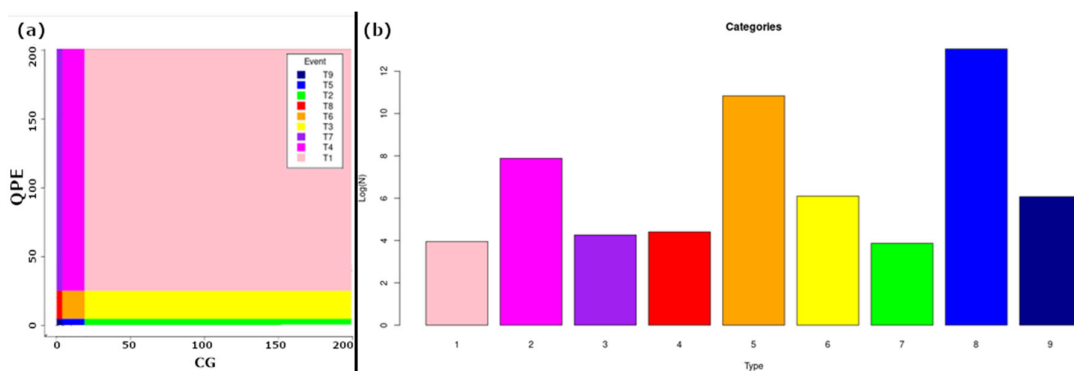


Figure 6. (a) Type event categorization according to daily values of QPE (y-axis) and CG flashes (x-axis). (b) Logarithmic distribution of the different categories (see figure 5 for the legend of each category).

Figures 7 and 8 show the monthly and hourly normalized distributions of types 2 and 3 events. For the monthly distribution, two distinct seasons are evident: a cool season (November to April) with fewer than three cases per month and a minimum in February. On the contrary, there is a warm season (May to October) with more than three cases per month. Notably, five or more monthly cases occurred from June to September, with a peak of nearly seven in September. In the hourly distribution, a relative maximum occurs between 0 and 1 UTC (four cases per hour), while a more prominent maximum occurs between 14 and 18 UTC, with over nine cases per hour and a peak of fourteen at 15 UTC. This pattern resembles severe weather events in Catalonia [64], offset by one month and one hour relative to hail cases.

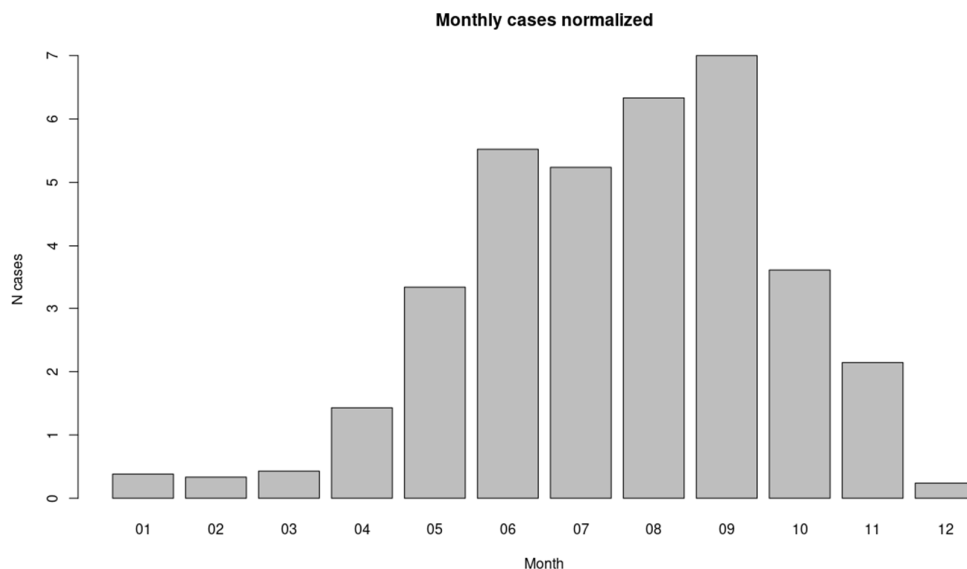


Figure 7. Monthly distribution (normalized per year) of types 2 and 3 events (RLR > 10 mm/CG) for the period 2006-2025.

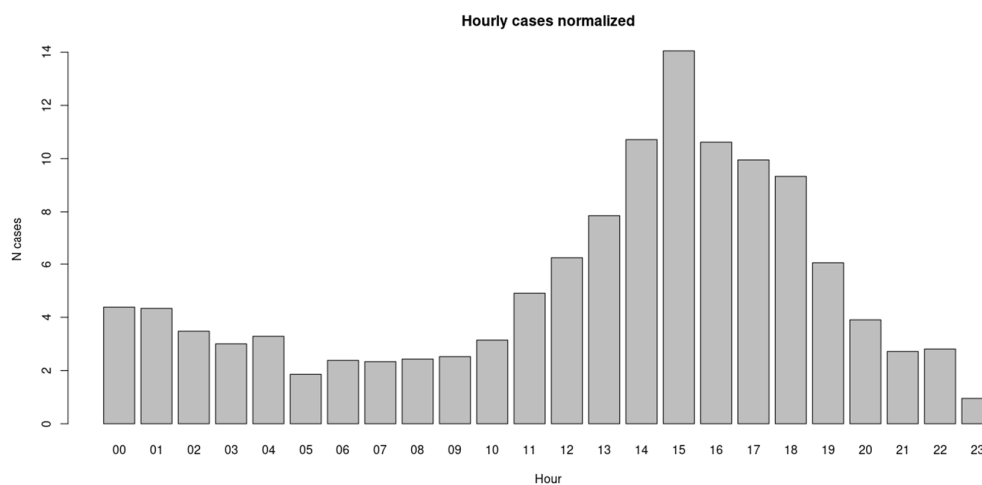


Figure 8. Hourly distribution (normalized per year) of types 2 and 3 events (RLR > 10 mm/CG) for the period 2006-2025.

The spatial distribution of hourly rainfall cases with RLR exceeding the 10 mm per flash (Figure 9) presents a gradient from coastal to inland data, with three relevant regions: the southern area (marked with an "A"), the central coastal and surrounded area ("B" label), and the Southern part of the Eastern Pyrenees ("C" area). The first region has been analyzed in [65] due to the high number of flood events, indicating that in most cases the elevated cumulated values are accompanied by a high lightning density. However, most flashes are concentrated over the sea. Region C is very close to the hotspot of thunderstorms in Catalonia during the Summer [66], and the monthly events distribution is slightly different from that shown in Figure 7, with most cases occurring in July and August, followed by June and September. During the rest of the year, the number of events is negligible. Finally, the Southern part of Region B was analyzed from the viewpoint of radar structures in [67]. In the present Research, we focus on the complete area of Region B, analyzing other meteorological fields to improve our understanding, as presented in [65].

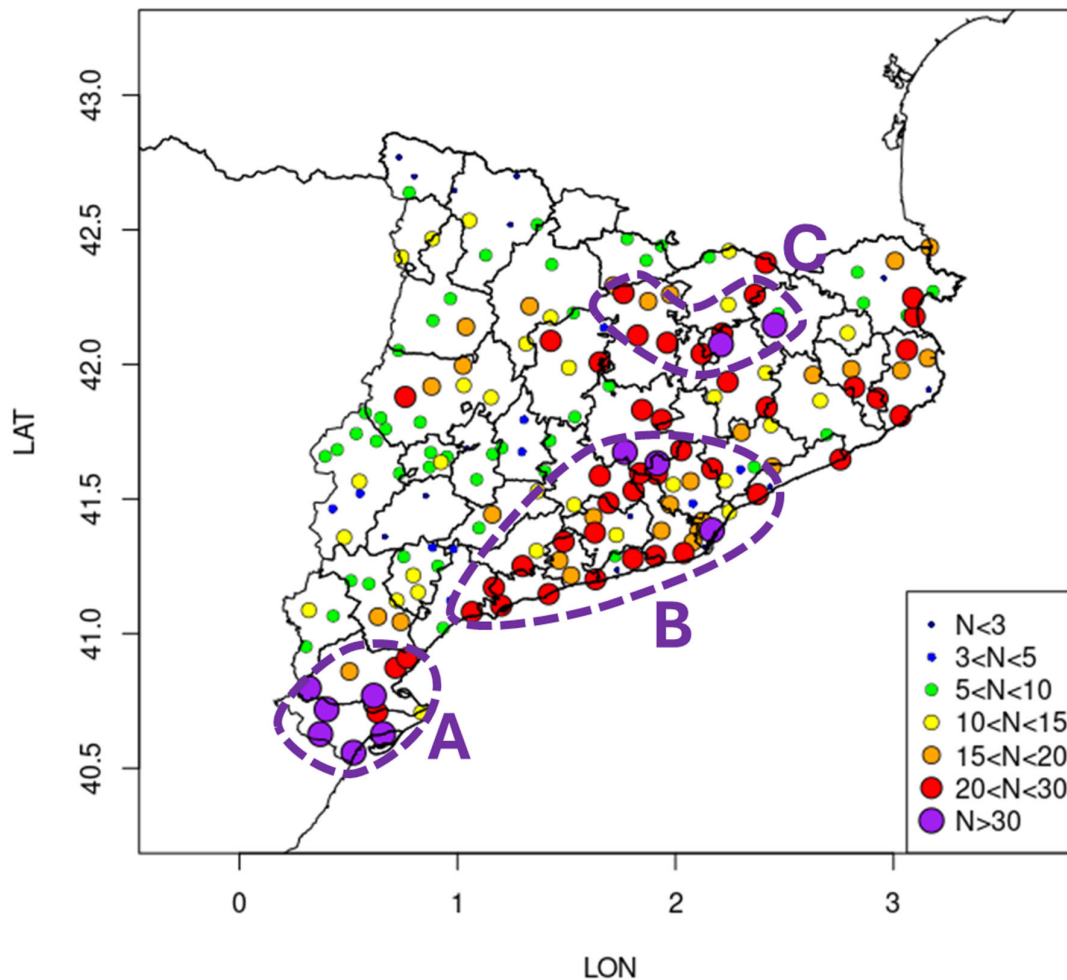


Figure 9. Spatial distribution of types 2 and 3 ($RLR > 10$ mm/CG) events for the period 2006-2025. The purple dotted lines delimitate the three main areas with this kind of cases (highly efficient with low or null lightning activity): the Southern area (Ebre Delta and surroundings, labelled with an “A”), the Central Coast and the neighboring inland region (labeled “B”), and the Eastern Pyrenees (labeled “C”).

4.2. Trends of RLR

Figure 10 presents the yearly distribution of warm rain events with RLR over 10 mm/CG. The first characteristic is the irregularity of events in consecutive years. In this sense, the best example is observed between 2017 and 2018, and between 2018 and 2019. Meanwhile, 2018 presented the maximum value of cases (67); the other two years had the lower values of the period (16 and 21 cases, respectively). The irregularity can also be observed in the fact that only five years have close values (a difference of less than three) to the mean 37.8 (black line). The second point of interest is the existence of an increasing trend in the number of cases per year, despite the irregularity. Considering the entire period, the trend (red line) shows an increase of 0.28 cases per year ($R^2 = -0.03$). However, if we remove the central years of the period (2015 and 2016), which show a decreasing trend, we can observe two nine-year periods (2006-2014 and 2017-2025) with increasing trends of 1.77 and 1.35 cases per year ($R^2 = 0.26$ and -0.08), respectively.

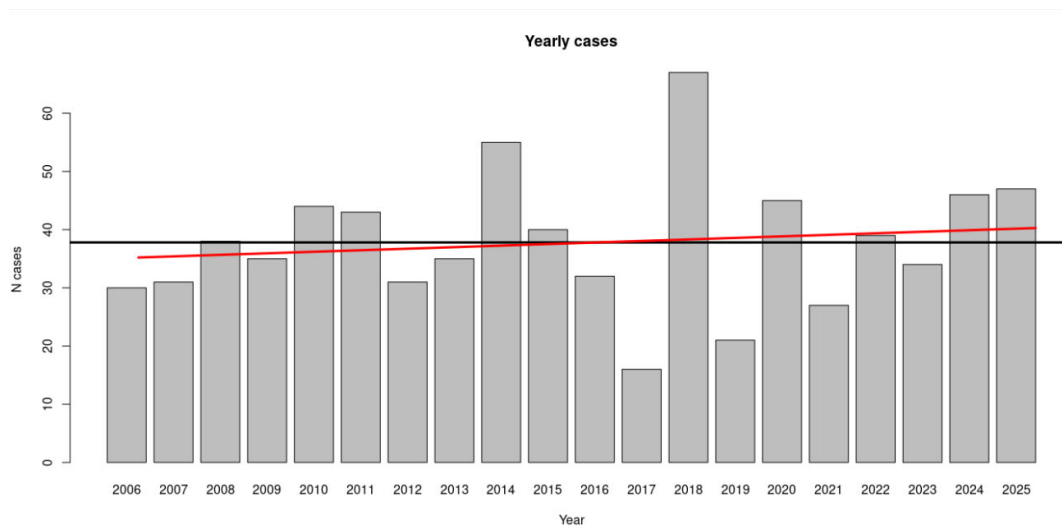


Figure 10. Yearly distribution of types 2 and 3 (RLR > 10 mm/CG) events for the period 2006-2025. Black line is the mean. Red line is the trend.

4.3. Presentation of Some Cases of Interest

The selected events have been considered due to different signatures. First, they have a notable impact in some cities on the Central Coast and the surrounding region. In all cases, there were some local floods. Figure 11 shows an example of a street flood during the event of 2 September 2019. According to Llasat et al. [68,69], floods in Catalonia are classified in three categories: extended floods (lasting for one week with total precipitation exceeding 200 mm in several areas), extended flash-floods (lasting for one day to one week with total precipitation exceeding 200 mm in a localized area, with punctual values over the 300 mm), and local flash floods (less than 1 day, but in general less than 3 hours, and precipitation rarely exceeding the 100 mm in a very small area). All the events presented here can be included in the last type of the previous classification.



Figure 11. Container swept away by the water current after an intense warm rain episode in Badalona on 2 September 2019. The nearest AWS (Badalona-Museu) recorded 17.3 mm in total, 13.2 mm in 30 minutes, and 0.8 mm in 1 minute of rainfall. The huge quantity of water flowing over the street suggests the core of the shower fell far from the AWS. Two hours later, another heavy rain developed at Viladecans (Figure 2.b), which registered higher values of rain than in Badalona, up to 40.7 mm in 30 minutes of rainfall (event A from Table 2). Picture from a video from Oriol Rodríguez (2019): <https://x.com/i/status/1168624146286305282>.

4.4. Precipitation Characteristics

The episodes of warm rain in Catalonia are caused by small vertical and horizontal clouds, such as shallow cumulus convection. The small magnitude of warm rain-producing clouds means that remote sensing tools don't usually diagnose their intensity adequately. This is because they have a shape of simple, warm, shallow, and low clouds, with no or little lightning, as Hawaiian warm rain showers. Meanwhile, radar images show local and small nuclei of moderate to heavy reflectivity with 1 km CAPPI maximum reflectivity oscillating between 45 and 55 dBZ. Besides, echotops (TOP12 dBZ) usually get 4-6 km ASL. Moreover, because of their small dimensions and scattered distribution (Figure 12), showers usually don't rain over the rain gauges. It makes the precipitation registered from automatic weather stations hardly reflect the reality because the maximum is usually concentrated in small areas, often far from rain gauges.

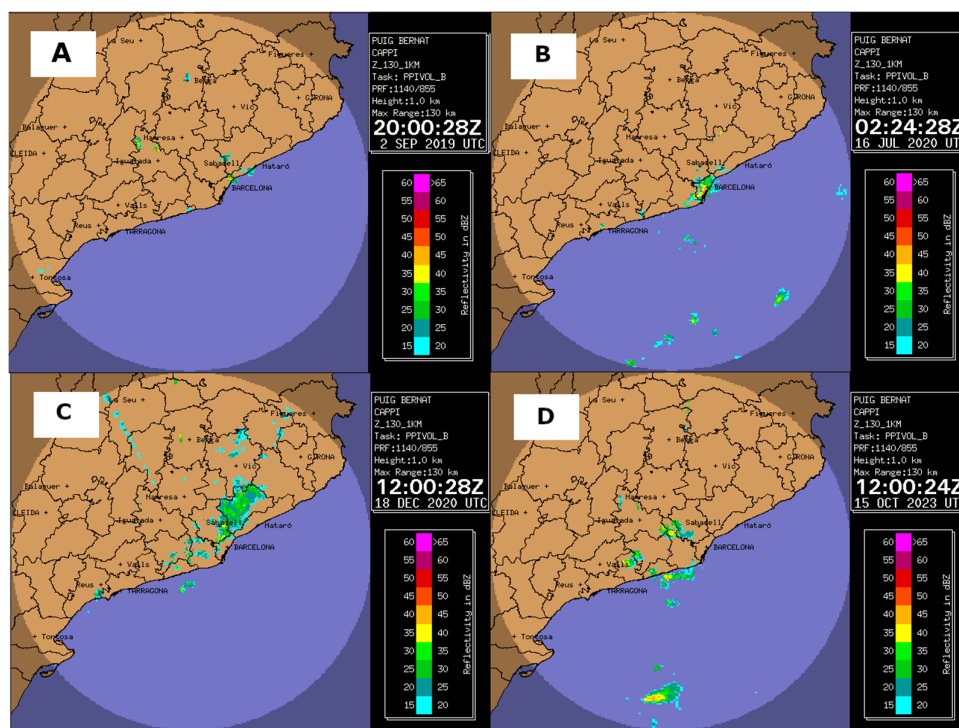


Figure 12. Examples of precipitation structures during the four heavy rain events of Table 2. Except in case (c), all the events show small scattered nucleus of moderate to high reflectivity.

Anyway, if we take a close look, we will find out interesting features. The heavy showers that finally fall over a rain gauge can register substantial amounts of precipitation in a day, from 40 to 70 mm (Table 2). However, those values exceeded 100 mm in 24 hours in specific cases. It was the case of 18th December 2020, when at Cerdanyola del Vallès (Figure 2.b), fell 273,6 mm fell in one day (Table 2); meanwhile, at Sant Cugat del Vallès, a town only 3 km west of Cerdanyola del Vallès, recorded 93,3 mm in the same period, with 30 minutes and 1 minute rainfall of 12,6 mm and 1,0 mm respectively.

In any case, the main characteristic of these episodes is their high rainfall rate. Usual values are from 15 to 40 mm in 30 minutes and from 0.5 to 2.7 mm in only 1 minute (Table 2). However, there are exceptions, such as the early morning of 16 July 2020, when Barcelona-el Raval AWS recorded 52.3 mm in only 30 minutes, with a 1-minute maximum rainfall rate of 2.7 mm. Such high rainfall rates can cause flash floods, as in Figure 11. Finally, during warm rain events in Catalonia, no hail is observed, as occurs in Hawaiian showers [38], the Fort Collins flash flood [33], and the Madison County flash flood [45].

Table 2. Precipitation recorded in the automatic weather station from XEMA during four heavy warm rain episodes. In the case of Cerdanyola del Vallès, it was registered by a Hellman rain gauge. (*) 30-minute and 1-minute rainfall were recorded at the AWS of Sant Cugat del Vallès, located 3 km northeast of Cerdanyola del Vallès. Sant Cugat del Vallès registered 93,3 mm during the event.

Event	Date	Location	24-Hours Rainfall (mm)	30-min. Rainfall (mm)	1-Min. Rainfall (mm)
A	2 September 2019	Viladecans	42,2	40,7	2,5
B	16 July 2020	Barcelona	66,3	52,3	2,5
C	18 December 2020	Cerdanyola del Vallès	273,6	12,6 ^(*)	1,0 ^(*)
D	15 October 2023	els Hostalets de Pierola	41,3	32,9	2,8

4.5. The Synoptical Environment

The four events of warm rain studied occur after a trough or a cold front crosses the area of interest. Once any of these two structures has crossed Catalonia, a small ridge, or in a few cases the zonal flow, comes close to the region (Figure 14). Consequently, a subsidence inversion (Figure 15), with very dry air aloft, forms over the vertical of the region at low-mid tropospheric levels, around 3000-4000 meters ASL. This inversion efficiently limits the growth of convective clouds. At the same time, an anticyclone usually approaches from the Atlantic Ocean (Figure 13). It makes the wind turn to the north and northwest. The interaction of these fourth-quadrant winds with topography generates the Pyrenean Wake (Figure 1) that drags humidity and heat from the Mediterranean Sea.

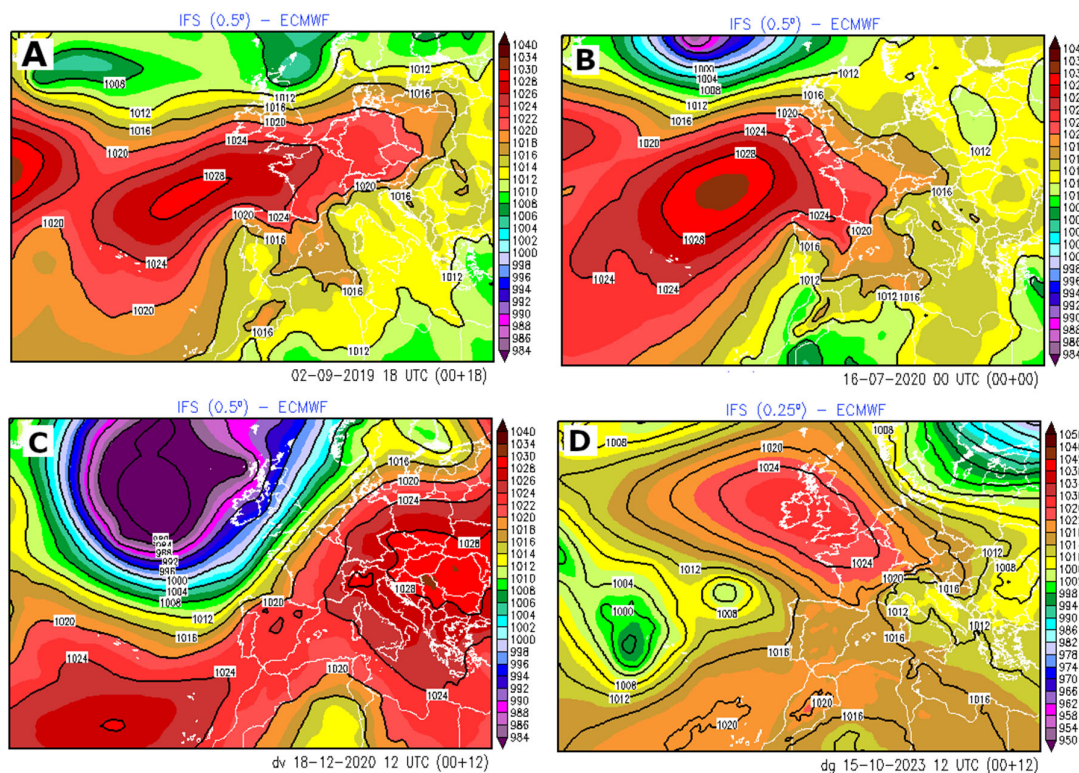


Figure 13. Pressure field at the surface from the IFS of ECMWF. The maps are plotted at the same time as the event or 3 h before. The North of the Iberian Peninsula is under the influence of a high-pressure zone, which lets northwestern and northern winds arrive at Catalonia from the Ebro Valley and the Gulf of Lion, respectively, and develop the Pyrenean Wake. In case (d), northern winds only affect the northeast edge of Catalonia. In case (c), northern winds are nonexistent; however, easterly winds also arrive at the coast, bringing moist and warm air mass likewise.

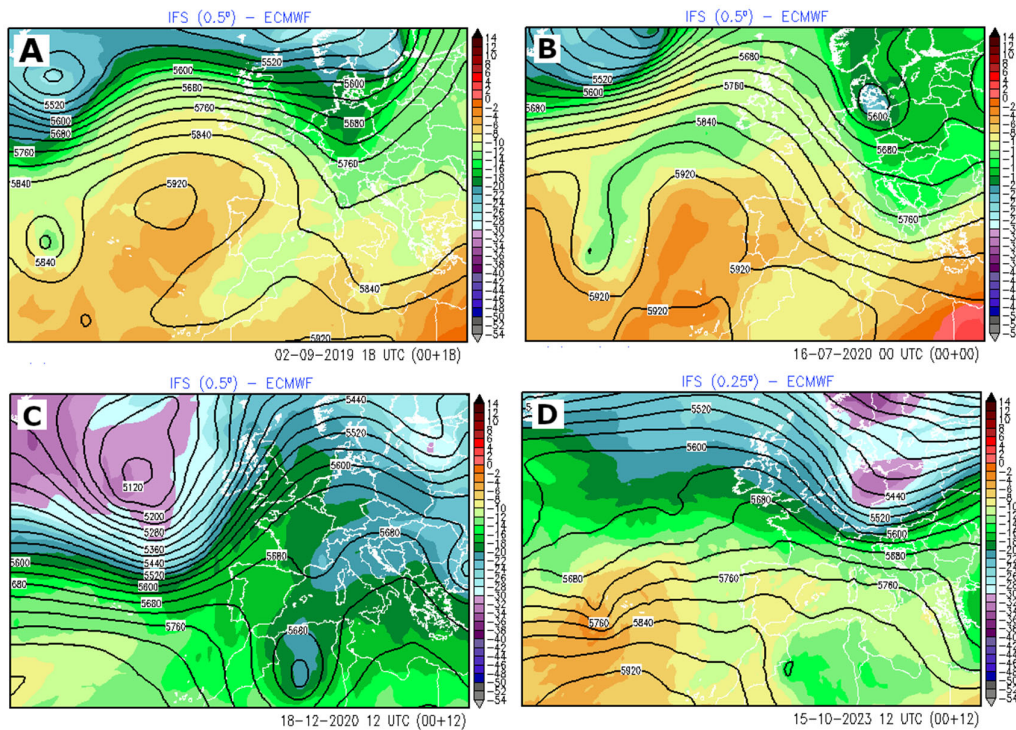


Figure 14. Geopotential (m) and temperature ($^{\circ}\text{C}$) at 500 hPa from IFS of ECMWF. The maps are plotted at the same time as the event or 3 h before. In all the events, a trough has just crossed Catalonia, and behind it a small or wide ridge approaches from the west. In case (d), these structures are quite subtle.

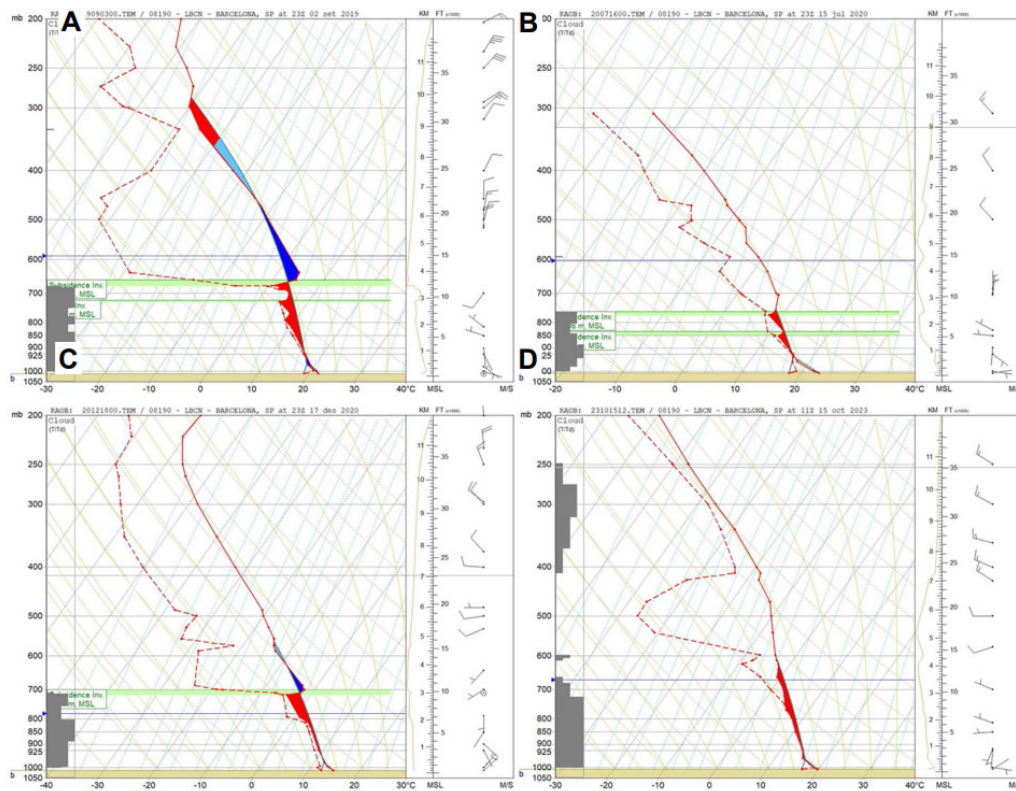


Figure 15. Skew-T/Log-P sounding analysis, created with the RAOB program, from Barcelona Sounding Station (WMO code 08190) for the four warm rain events, is shown in Table 2. All the soundings aren't modified. The

red shaded area is CAPE, the dark blue shaded area is CIN, the horizontal solid blue line is freezing level, the horizontal green shaded lines are subsidence inversions, the grey shaded area in the left column is cloudiness, and the brown-orange line in the right column is Equivalent Potential Temperature (without unit).

4.6. Mesoscale and Thermodynamics

The warm rain episodes analyzed here are directly related to the Mediterranean air mass. It is in this maritime warm and humid air mass, which northern and northwestern winds cannot sweep, that the events studied develop. Therefore, the main features to highlight are the characteristics of the air mass that remains in the central coast and pre-coastal area from mesoscale and thermodynamic perspectives, as well as different convergence lines that form along it.

The analysis of the vertical wind profile reveals between southerly and easterly flow up to around 1 km ASL (Figure 15), which ensures the entrance of a very humid air mass (Figures 16 and 17). In fact, 0-3 km mean relative humidity oscillates between 83 and 94%, while the 850 hPa dew point depression is almost always below the 1 °C level. Consequently, the atmospheric PWC is relatively high (oscillates between 2,5 and 3,5 cm), and it's a basic ingredient for the occurrence of heavy and abundant precipitation according to [11,70]. This high humidity also explains the low cloud bases, situated between 400-700 meters ASL (Table 2). Freezing level oscillates from 2800 up to 4200 meters ASL, so most or all the cloud extends below the 0 °C level. The freezing level gets higher altitudes during the summer and early autumn, and approaches the tropical freezing level values, which oscillate between 4 and 6 km ASL [71]. Consequently, combining a high freezing level with a low cloud base creates a deep warm cloud layer. In this layer, the coalescence or warm rain process can occur, which increases the efficiency, rainfall rate, and accumulation [11,34].

It is interesting to note that all this saturated or subsaturated profile is built underneath the thermal inversion at low-mid tropospheric levels, around 3000-4000 meters ASL (or between 700-600 hPa). Upon the inversion level, the air is very dry, and the wind turns to a moderate westerly or northerly wind. That inversion, as well as the saturated air below and the dry air over it, is common in other warm rain events around the world [12,38]. The EL usually coincides with the inversion height. The presence of the inversion limits cloud growth (Figure 18). And thus, it prevents warm and moist updrafts from ascending much over the freezing level, where the formation of ice would probably initiate the thunderstorm electrification process. In a few cases, the thermal inversion doesn't form clearly; instead, a slight decrease of the vertical lapse rate works as an inversion (Figure 15, case D).

The thermodynamic environment reveals low values of instability indices. For instance, total CAPE oscillates from 80 to 300 J/kg. These values are similar to those observed in other warm rain events [33]. Most values of LI [72] are between +3 and 0; meanwhile, the majority of TT [72] oscillates between 41 and 46. In addition, a remarkable feature of these events is that most of the CAPE and PWM are concentrated below the thermal inversion height (Table 2).

Another feature to emphasize is the convergence lines necessary to trigger the formation of the swallow cumulus. Northern (Tramuntana) and northwestern (Mestral) dry and cold winds turn prominently to their right and left, respectively, when they reach the Mediterranean Sea. After travelling some tens of kilometers over the Mediterranean Sea, they drag heat and humidity from the sea, so they become warm and moist winds (Figure 17 panels (a), (b), (d), and Figure 1a). Finally, they arrive at the coast as southern and/or eastern winds, which converge in the central area of the Catalan Coast.

But convergence lines are also caused by other mechanisms. In some cases, the convergence is due to the interaction of these southern or eastern winds with either the Litoral or Prelitoral mountain ranges. In other cases, convergence occurs when the nocturnal land breeze coincides with low-level southerly and easterly winds. This causes the occurrence of convection offshore or just over the coast. A convergence line over the sea is also documented at Sumatra's western coast [73].

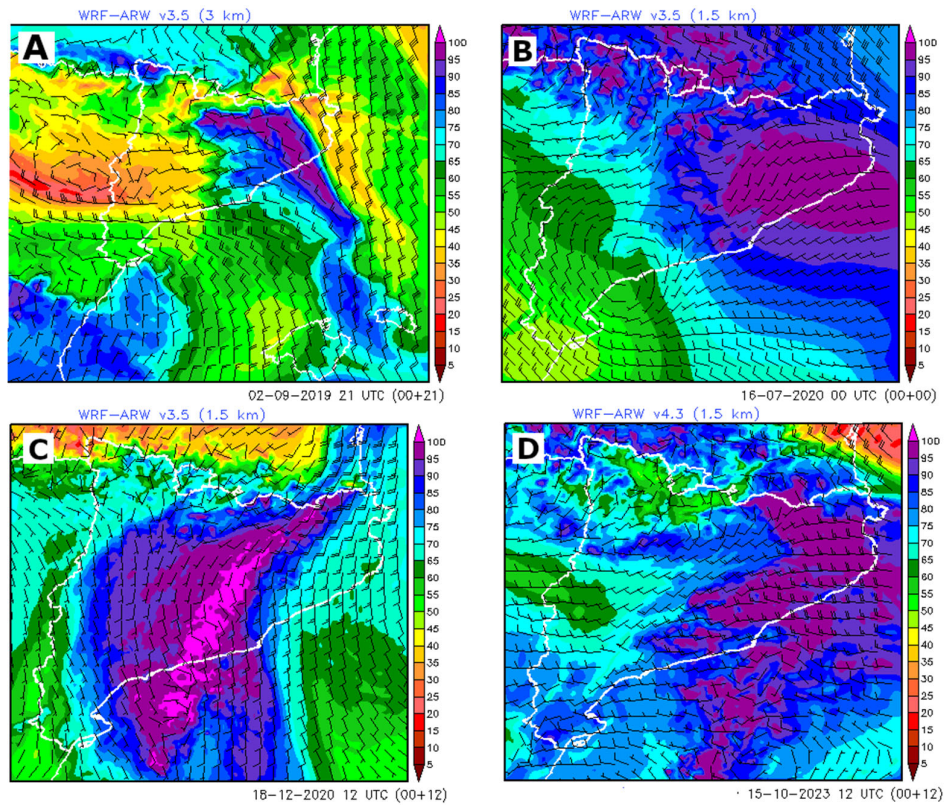


Figure 16. Relative humidity (%) and wind (kt) at 850 hPa for the WRF model for the four warm rain events. In all cases, a wide or sometimes narrow saturated air mass is present in the eastern part of Catalonia at this altitude.

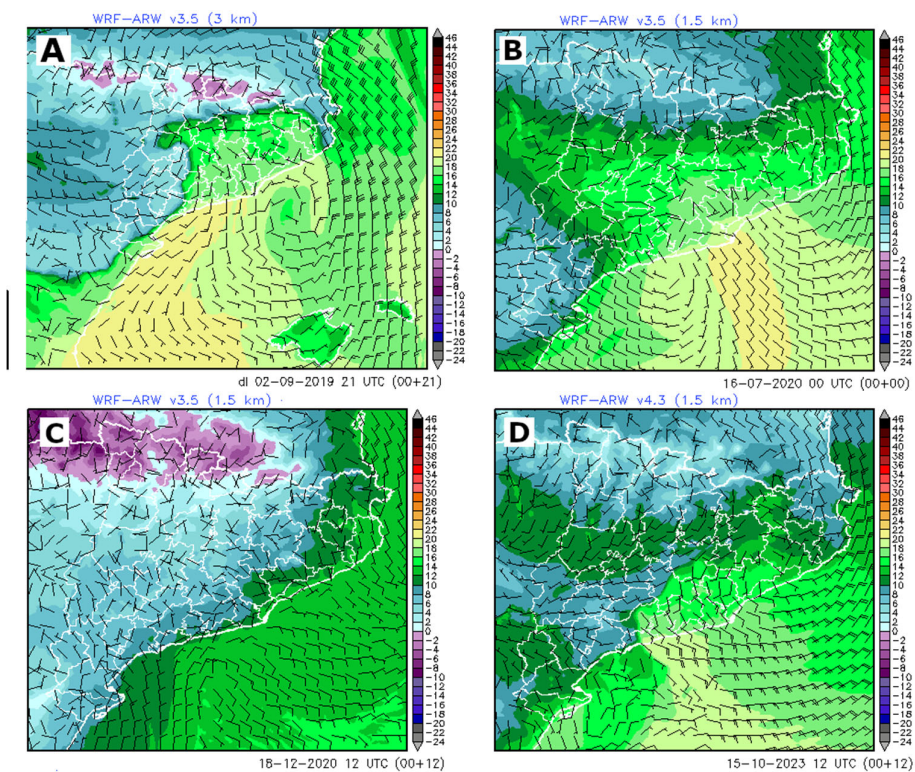


Figure 17. Dew point temperature (°C) and wind (kt) at the surface for the WRF model. The presence of higher values of surface dew point temperature (relative to the surrounding area) at the central part of the litoral and

prelitoral reveals the inshore entrance of a humid and warm air mass from the Mediterranean Sea. In addition, in maps a), b), and d), the bearing of Tramuntana wind to eastern or southern winds is clearly noticeable, bringing to light the Pyrenean Weak. On the contrary, in map c), there is no northern wind, but it maintains the maritime origin of the air mass.

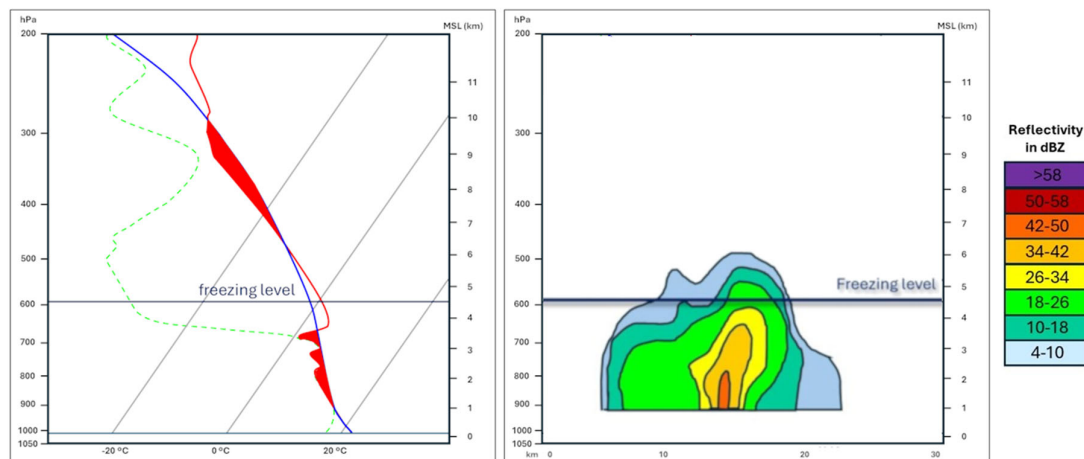


Figure 18. Conceptual model of the radio-sounding thermodynamic profile (left) and vertical radar section (right) of the warm rain events in Catalonia.

4.7. The Conceptual Model

Based on the previous results, we propose a conceptual model of this type of event focusing on the radio-sounding thermodynamic profile and the radar vertical structure (Figure 18). Besides, Table 2 provides some reference values for the rainfall characteristics, radar fields (reflectivity and TOP12), and the most relevant thermodynamic parameters.

Table 2. Reference values for warm convective rainfall events in Catalonia.

Variable	Range values
24-hours accumulation	From 20 to 70 mm
30 minutes rainfall rate	From 15 to 40 mm
Maximum reflectivity (CAPPI 1 km)	From 45 to 55 dBZ
TOP12 dBZ	From 4 to 6 km ASL
850 hPa temperature	From 7 to 12 °C
850 hPa dew point depression	Below 1 °C
Freezing level	From 2800 to 4200 meters ASL
CAPE total	From 80 to 300 J/kg
EL	From 3000 to 4000 meters ASL (or 700-600 hPa)
LCL	From 400 to 700 meters ASL
LI	From 0 to +3
PWM	From 2,5 to 3,5 cm
TT	From 41 to 46

5. Discussion

This study analyses warm rain events, a type of precipitation that affects coastal and pre-coastal regions of Catalonia. This territory is widely inhabited and urbanized, including small and narrow stream basins that have short hydrological responses. These episodes are characterized by high-efficiency precipitation that produces high rainfall rates. Furthermore, substantial amounts of precipitation can also be registered. In a few cases, the usual values were exceeded, registering more

than 100 mm in one day. But, as mentioned before, what makes these events a threat is their high rainfall rate. Therefore, the combination of high population density, high rainfall rate, and flash floods turns warm rain events into a hazard for people and infrastructures.

In comparison to other warm convective rain around the world, the episodes studied in this paper share some characteristics with them. For instance, maximum values of radar reflectivity are concentrated in the bottom part of the cloud within the warm portion of the cloud layer, which is known as Low Echo Centroid (LEC) [11,33,74]. Furthermore, all these events occurred in a moist and warm maritime airmass. This fact is independent of whether they develop over the sea, inshore, or far away from the sea [33,39,45].

The thermal inversion present in these episodes is around 700-600 hPa, or 3000-4000 meters ASL. This is the limiting height of the cloud top. Although it is at a little higher altitude, it aligns with other documented warm rain events, as in Valentia (Ireland) and San Antonio (USA) [12], as well as in the Hawaii islands [39], where the thermal inversion stops the growth of the clouds, whose tops fluctuate between 2000 and 3500 meters above sea level. Nevertheless, not all heavy warm rain events around the world exhibit an inversion, allowing clouds to develop up to the upper troposphere (from 10 to 13 km height, or even higher) [11,33,74,75].

In this way, Catalan warm rain events have very low values of instability indices (e.g., CAPE from 80 to 300 J/kg or LI greater than 0). These values are notably low compared with warm rain in other regions. Those cases have instability indices such as CAPE higher than 850 J/kg and LI lower than -2 [11,33,74]. In addition, in Catalan warm rain events, CAPE and PWM are concentrated in the lower troposphere. On the other hand, these magnitudes are distributed along the troposphere in the other cases.

The NWP models were and are limited in modeling accurate atmospheric conditions linked to the Catalan WCR. The limitations are higher in the case of synoptic models. The reasons are mainly the grid size and the simplistic configuration of the parametrization. Mesoscale models provide better results, but forecasts of events are only available within a few days (sometimes only a few hours), and with a high uncertainty regarding the location and quantity of the showers.

This uncertainty is also reflected in synthetic vertical profiles: if the model cannot accurately forecast all the atmospheric levels, it would not provide a good location for the rainfall field. Furthermore, the comparison of these forecasted vertical conditions with the real ones is limited by the fact that only one sounding point (Barcelona) is available (at 00 and 12 UTC). Therefore, if the instability is far from this point, the sounding would not reproduce the real conditions of the atmosphere.

Observations of the events are limited by the short areas affected by the rainfall. In most cases, the rain gauges rarely describe the behavior of the event because they are far from the maximum. Even the high increase in stations has not avoided this complexity. However, the combination of rain gauges with radar fields has resulted in useful mitigation of the issue, but not in all situations and locations. Depending on the vertical development of the rainfall cloud, the radar can accurately detect precipitation or not. Therefore, the diagnosis result will be satisfactory or not.

To end, future work would focus on two main goals. On the one hand, we need to improve our knowledge and understanding of these events. On the other hand, we should get better recognition during operational surveillance tasks. Regarding knowledge, future work should focus on the role analysis of three different variables. These magnitudes are the dew point, the equivalent potential temperature at low altitudes, and the SST. Furthermore, the relationship between SST and temperature at 850 hPa should also be understood more deeply. Finally, warm cloud depth [11] should be analyzed to forecast air masses associated with heavy warm rain events. From an operational viewpoint, we should improve the identification of the LEC radar signature. Moreover, the use of cloud phase images from Meteosat Third Generation can help us recognize these clouds better than in the past. However, the objective should be to establish an automatic detection system of warm rain events that can help in surveillance tasks to anticipate high rainfall rates. In this sense,

techniques such as neuronal networks, ensembles, or other artificial intelligence methodologies could be used to detect relevant factors in model fields and remote sensing data.

6. Conclusions

This study presents an analysis of warm rain events, a type of common but quite unknown heavy rain episode in Catalonia.

These episodes are characterized by highly efficient precipitation that produces large rainfall rates. They appear throughout the year, although events with higher rainfall usually occur during summer and autumn. There are no dynamic forcing features at upper tropospheric levels. Despite this, relevant factors are found at lower atmospheric levels, such as local wind convergences, a thermal inversion at low and medium troposphere, and a saturated airmass with elevated atmospheric precipitable water below this inversion. The thermodynamic profile is the most important predictor of warm rain events, although the environment reveals only low values of instability concentrated at the bottom of the profile. These events are difficult to follow with surveillance tools. Anyway, radar data is the most useful remote sensor tool for these tasks.

In any case, the consolidation of the conceptual model, advancements in monitoring tools, and improved mesoscale models have strengthened the forecasters' capabilities to identify these events. Consequently, they can issue heavy precipitation warnings with greater accuracy and timeliness.

Author Contributions: Conceptualization, F.F. and D.B.; methodology, F.F. and D.B.; formal analysis, F.F. and D.B.; investigation, F.F. and D.B.; resources, M.A.; data curation, T.R.; writing—original draft preparation, F.F.; writing—review and editing, F.F., D.B. and T.T.; visualization, F.F. and T.R.; supervision, M.A.; All authors have read and agreed to the published version of the manuscript.

Funding: This research received no external funding.

Institutional Review Board Statement: Not applicable.

Informed Consent Statement: Not applicable.

Data Availability Statement: Data files are available under requirement via e-mail, and they are only considered for research purposes.

Acknowledgments: The authors want to thank the Servei Meteorològic de Catalunya for facilitating the research, and in special to the Equip de Predicció i Vigilància for their useful comments and suggestions.

Conflicts of Interest: The authors declare no conflicts of interest.

Abbreviations

The following abbreviations are used in this manuscript:

AMP	Amposta sensor
ASL	Above Sea Level
CAPE	Convective Available Potential Energy
CIN	Convective Inhibition
CAPPI	Constant Altitude Plan Position Indicator
CG	Cloud-to-ground
CCR	Cold Convective Rainfall
CTT	Cloud-top temperature
ECMWF	European Center for Medium-Range Weather Forecasts
EL	Equilibrium Level
CG	Cloud to ground (flash)
EPV	Equip de Predicció i Vigilància (in Catalan, Forecasting and Surveillance Team)
FRZG	Freezing Level
GAC	Globa Atmospheric Circulation

GFS	Global Forecast System
GME	Global Model
GSM	Global System for Mobile communications
IC	Intra-cloud (lightning)
IR	Infrared
LCL	Lifted Condensation Level
LEC	Low Echo Centroid
LF	Low Frequency
LI	Lifted Index
LMI	La Miranda radar
MM5	Fifth-Generation Penn State/NCAR Mesoscale Model
MSG	Meteosat Second Generation
NWP	Numerical Weather Prediction Models
PPI	Plan Position Indicator
PWM	Precipitable Water Mass content
RLR	Rainfall-Lightning-Relationship
SMC	Servei Meteorològic de Catalunya (in Catalan, Meteorological Service of Catalonia)
SST	Sea Surface Temperature
TOP12	The echo top exceeding the 12 dBZ reflectivity threshold in radar imagery
TRMM	Tropical Rain Measurement Mission
TT	Total Totals Index
VHF	Very High Frequency
WCR	Warm Convective Rain
WL	Warm Layer
WMO	World Meteorological Organization
WR	Warm Rain
WRF	Weather Research and Forecasting
XDDE	Xarxa De Descàrregues Elèctriques (in Catalan, Lightning Detection Network)
XEMA	Xarxa d'Estacions Meteorològiques Automàtiques (in Catalan, Automatic Weather Stations Network)
XRAD	Xarxa de Radars Meteorològics (in Catalan, SMC Radar Network)

References

1. Prein, A.F., and Heymsfield, A.J. (2020) Increased melting level height impacts surface precipitation phase and intensity. *Nat. Clim. Chang.* **10**, 771–776. <https://doi.org/10.1038/s41558-020-0825-x>
2. Blyth, A. M., Lowenstein, J. H., Huang, Y., Cui, Z., Davies, S., & Carslaw, K. S. (2013). The production of warm rain in shallow maritime cumulus clouds. *Quarterly Journal of the Royal Meteorological Society*, **139**(670), 20-31, <https://doi.org/10.1002/qj.1972>.
3. Kodama, Y. M., Katsumata, M., Mori, S., Satoh, S., Hirose, Y., & Ueda, H. (2009). Climatology of warm rain and associated latent heating derived from TRMM PR observations. *Journal of climate*, **22**(18), 4908-4929, <https://doi.org/10.1175/2009JCLI2575.1>.
4. Beard, K. V., & Ochs III, H. T. (1993). Warm-rain initiation: An overview of microphysical mechanisms. *Journal of Applied Meteorology and Climatology*, **32**(4), 608-625, [https://doi.org/10.1175/1520-0450\(1993\)032<0608:WRIAOO>2.0.CO;2](https://doi.org/10.1175/1520-0450(1993)032<0608:WRIAOO>2.0.CO;2).
5. Atlas, D., & Ulbrich, C. W. (2000). An observationally based conceptual model of warm oceanic convective rain in the tropics. *Journal of Applied Meteorology*, **39**(12), 2165-2181., [https://doi.org/10.1175/1520-0450\(2001\)040<2165:A0BCMO>2.0.CO;2](https://doi.org/10.1175/1520-0450(2001)040<2165:A0BCMO>2.0.CO;2).
6. Battaglia, A., Kollias, P., Dhillon, R., Lamer, K., Khairoutdinov, M., & Watters, D. (2020). Mind the gap—Part 2: Improving quantitative estimates of cloud and rain-water path in oceanic warm rain using spaceborne radars. *Atmospheric Measurement Techniques*, **13**(9), 4865-4883, <https://doi.org/10.5194/amt-13-4865-2020>.
7. Lau, K. M., & Wu, H. T. (2003). Warm rain processes over tropical oceans and climate implications. *Geophysical Research Letters*, **30**(24), <https://doi.org/10.1029/2003GL018567>.

8. Ikeda, K., Rasmussen, R. M., Brandes, E., & McDonough, F. (2009). Freezing drizzle detection with WSR-88D radars. *Journal of applied meteorology and climatology*, 48(1), 41-60, <https://doi.org/10.1175/2008JAMC1939.1>.
9. Rauber, R. M., Olthoff, L. S., Ramamurthy, M. K., & Kunkel, K. E. (2000). The relative importance of warm rain and melting processes in freezing precipitation events. *Journal of Applied Meteorology*, 39(7), 1185-1195, [https://doi.org/10.1175/1520-0450\(2000\)039<1185:TRIOWR>2.0.CO;2](https://doi.org/10.1175/1520-0450(2000)039<1185:TRIOWR>2.0.CO;2).
10. Nelson, L. D. (1971). A numerical study on the initiation of warm rain. *Journal of Atmospheric Sciences*, 28(5), 752-762, [https://doi.org/10.1175/1520-0469\(1971\)028<0752:ANSOTI>2.0.CO;2](https://doi.org/10.1175/1520-0469(1971)028<0752:ANSOTI>2.0.CO;2).
11. Davis, R. S. (2004). The impact of tropical rainfall rates on flash flood detection. In *Preprints, 22nd Conf. on Severe Local Storms*, Hyannis, MA, Amer. Meteor. Soc. B, 11.
12. Ohtake, T. (1963). Hemispheric investigation of warm rain by radiosonde data. *Journal of Applied Meteorology* (1962-1982), 594-607, [https://doi.org/10.1175/1520-0450\(1963\)002<0594:HIOWRB>2.0.CO;2](https://doi.org/10.1175/1520-0450(1963)002<0594:HIOWRB>2.0.CO;2).
13. Huffman, G. J., & Norman Jr, G. A. (1988). The supercooled warm rain process and the specification of freezing precipitation. *Monthly weather review*, 116(11), 2172-2182., [https://doi.org/10.1175/1520-0493\(1988\)116<2172:TSWRPA>2.0.CO;2](https://doi.org/10.1175/1520-0493(1988)116<2172:TSWRPA>2.0.CO;2).
14. Kodama, K., & Barnes, G. M. (1997). Heavy rain events over the south-facing slopes of Hawaii: Attendant conditions. *Weather and forecasting*, 12(2), 347-367, [https://doi.org/10.1175/1520-0434\(1997\)012<0347:HREOTS>2.0.CO;2](https://doi.org/10.1175/1520-0434(1997)012<0347:HREOTS>2.0.CO;2).
15. Liu, C., Zipser, E. J., Cecil, D. J., Nesbitt, S. W., & Sherwood, S. (2008). A cloud and precipitation feature database from nine years of TRMM observations. *Journal of Applied Meteorology and Climatology*, 47(10), 2712-2728, <https://doi.org/10.1175/2008JAMC1890.1>.
16. Liu, C., & Zipser, E. J. (2009). "Warm rain" in the tropics: Seasonal and regional distributions based on 9 yr of TRMM data. *Journal of Climate*, 22(3), 767-779, <https://doi.org/10.1175/2008JCLI2641.1>.
17. Suzuki, K., & Stephens, G. L. (2009). Relationship between radar reflectivity and the time scale of warm rain formation in a global cloud-resolving model. *Atmospheric research*, 92(4), 411-419, <https://doi.org/10.1016/j.atmosres.2008.12.010>.
18. Doswell III, C. A., Ramis, C., Romero, R., & Alonso, S. (1998). A diagnostic study of three heavy precipitation episodes in the western Mediterranean region. *Weather and Forecasting*, 13(1), 102-124, [https://doi.org/10.1175/1520-0434\(1998\)013<0102:ADSOTH>2.0.CO;2](https://doi.org/10.1175/1520-0434(1998)013<0102:ADSOTH>2.0.CO;2).
19. Barnolas, M., & Llasat, M. C. (2007). A flood geodatabase and its climatological applications: the case of Catalonia for the last century. *Natural Hazards and Earth System Sciences*, 7(2), 271-281, <https://doi.org/10.5194/nhess-7-271-2007>.
20. Riesco, J., Tamayo, J., & Alcover, V. (2002). Heavy maritime rainfall in the Valencia Region: The 6 to 8 May 2002 situation. In *Proc. Fourth EGS Plinius Conf. on Mediterranean Storms*.
21. Martín, F., Elizaga, F., Carretero, O., and San, Ambrosio I. (2007). Diagnóstico y predicción de la convección profunda (in Spanish). Technical Note n. 35 of the Analysis and Forecasting Technical Service of the Spanish Weather Service, pp. 174.
22. Fullerton, C. M., & Raymond, D. J. (1973). WRRCTR No. 67 Rainfall Intensity Instruments and Measurements.
23. Nuijens, L., Stevens, B., & Siebesma, A. P. (2009). The environment of precipitating shallow cumulus convection. *Journal of the Atmospheric Sciences*, 66(7), 1962-1979, <https://doi.org/10.1175/2008JAS2841.1>.
24. Rigo, T., Berenguer, M., & del Carmen Llasat, M. (2019). An improved analysis of mesoscale convective systems in the western Mediterranean using weather radar. *Atmospheric Research*, 227, 147-156, <https://doi.org/10.1016/j.atmosres.2019.05.001>.
25. Insua-Costa, D., Lemus-Cánovas, M., Miguez-Macho, G., & Llasat, M. C. (2021). Climatology and ranking of hazardous precipitation events in the western Mediterranean area. *Atmospheric Research*, 255, 105521, <https://doi.org/10.1002/joc.5301>.
26. Pineda, N., Rigo, T., Bech, J., & Soler, X. (2007). Lightning and precipitation relationship in summer thunderstorms: Case studies in the North-Western Mediterranean region. *Atmospheric research*, 85(2), 159-170, <https://doi.org/10.1016/j.atmosres.2006.12.004>.

27. Williams, E., Guha, A., Boldi, R., Christian, H., & Buechler, D. (2019). Global lightning activity and the hiatus in global warming. *Journal of Atmospheric and Solar-Terrestrial Physics*, **189**, 27-34., <https://doi.org/10.1016/j.jastp.2019.03.011>.
28. Romero, R., Doswell III, C. A., & Ramis, C. (2000). Mesoscale numerical study of two cases of long-lived quasi-stationary convective systems over eastern Spain. *Monthly Weather Review*, **128**(11), 3731-3751, [https://doi.org/10.1175/1520-0493\(2001\)129<3731:MNSOTC>2.0.CO;2](https://doi.org/10.1175/1520-0493(2001)129<3731:MNSOTC>2.0.CO;2).
29. Ballart, D., Figuerola, F., Aran, M., & Rigo, T. (2009). Analysis of warm convective rain events in Catalonia. Proceedings of the 11th Plinius Conference on Mediterranean Storms, 11, Plinius11-115, 2009.
30. Short, D. A., and K. Nakamura, 2000: TRMM radar observations of shallow precipitation over the tropical oceans. *J. Climate*, **13**, 4107–4124, [https://doi.org/10.1175/1520-0442\(2000\)013<4107:TROOSP>2.0.CO;2](https://doi.org/10.1175/1520-0442(2000)013<4107:TROOSP>2.0.CO;2).
31. Houze Jr, R. A., Rasmussen, K. L., Zuluaga, M. D., & Brodzik, S. R. (2015). The variable nature of convection in the tropics and subtropics: A legacy of 16 years of the Tropical Rainfall Measuring Mission satellite. *Reviews of Geophysics*, **53**(3), 994-1021, <https://doi.org/10.1002/2015RG000488>.
32. Rigo, T. (2023). Warm Rain Analysis from Remote Sensing Data in the Metropolitan Area of Barcelona for 2015–2022. *Hydrology*, **10**(7), 142, <https://doi.org/10.3390/hydrology10070142>
33. Petersen, W. A., Carey, L. D., Rutledge, S. A., Knievel, J. C., Doesken, N. J., Johnson, R. H., McKee, T.B., Haar, T.V. & Weaver, J. F. (1999). Mesoscale and radar observations of the Fort Collins flash flood of 28 July 1997. *Bulletin of the American Meteorological Society*, **80**(2), 191-216, [https://doi.org/10.1175/1520-0477\(1999\)080<0191:MAROOT>2.0.CO;2](https://doi.org/10.1175/1520-0477(1999)080<0191:MAROOT>2.0.CO;2).
34. Davis, R. S. (2001). Flash flood forecast and detection methods. In *Severe convective storms* (pp. 481-525). Doswell, C.A. (eds) Meteorological Monographs. American Meteorological Society, Boston, MA. https://doi.org/10.1007/978-1-935704-06-5_12.
35. Argence, S., Lambert, D., Richard, E., Chaboureau, J. P., & Söhne, N. (2008). Impact of initial condition uncertainties on the predictability of heavy rainfall in the Mediterranean: A case study. *Quarterly Journal of the Royal Meteorological Society*, **134**(636), 1775-1788, <https://doi.org/10.1002/qj.314>.
36. Dayan, U., Nissen, K., & Ulbrich, U. (2015). Atmospheric conditions inducing extreme precipitation over the eastern and western Mediterranean. *Natural Hazards and Earth System Sciences*, **15**(11), 2525-2544, <https://doi.org/10.5194/nhess-15-2525-2015>.
37. Zhang, F., Odins, A. M., & Nielsen-Gammon, J. W. (2006). Mesoscale predictability of an extreme warm-season precipitation event. *Weather and forecasting*, **21**(2), 149-166, <https://doi.org/10.1175/WAF909.1>.
38. Fullerton, C.M. and Wilson, SK. (1974). Some Characteristics of Hawaiian High-Intensity Rainfall. Water Resources Research Center Tech. Report No. 78, University of Hawaii, Honolulu, HI, 47 pp.
39. Takahashi, T. (1977). A study of Hawaiian warm rain showers based on aircraft observation. *Journal of Atmospheric Sciences*, **34**(11), 1773-1790, [https://doi.org/10.1175/1520-0469\(1977\)034<1773:ASOHWHR>2.0.CO;2](https://doi.org/10.1175/1520-0469(1977)034<1773:ASOHWHR>2.0.CO;2).
40. Alpert, L. (1955). Notes on warm-cloud rainfall. *Bulletin of the American Meteorological Society*, **36**(2), 64-68, <https://doi.org/10.1175/1520-0477-36.2.64>.
41. Castillo, S., Rigo, T., & Farnell, C. (2022). Can the Correlation between Radar and Cloud-to-Ground Daily Fields Help to Identify the Different Rainfall Regimes? The Case of Catalonia. *Atmosphere*, **13**(5), 808, <https://doi.org/10.3390/atmos13050808>.
42. Veloria, A., Wada, Y., Hirose, H., Kitahara, D., Hayashi, S., & Ushio, T. (2025). Introduction of Lightning into the GSMaP Rainfall Measurements through Optimized Power-Law Model. *Journal of Atmospheric and Oceanic Technology*, **42**(6), 637-656, <https://doi.org/10.1175/JTECH-D-24-0040.1>.
43. Vicente-Serrano, S. M., Beguería, S., López-Moreno, J. I., El Kenawy, A. M., & Angulo-Martínez, M. (2009). Daily atmospheric circulation events and extreme precipitation risk in northeast Spain: Role of the North Atlantic Oscillation, the Western Mediterranean Oscillation, and the Mediterranean Oscillation. *Journal of Geophysical Research: Atmospheres*, **114**(D8), <https://doi.org/10.1029/2008JD011492>.
44. Vilaclara, E. (2002). Situacions del nord-oest sobre Catalunya: l'estela pirinenca. (in Catalan) *Tethys: Journal of Mediterranean Meteorology and Climatology*, **2**(7).

45. Pontrelli, M. D., Bryan, G., & Fritsch, J. M. (1999). The Madison County, Virginia, flash flood of 27 June 1995. *Weather and forecasting*, **14**(3), 384-404, [https://doi.org/10.1175/1520-0434\(1999\)014<0384:TMCVFF>2.0.CO;2](https://doi.org/10.1175/1520-0434(1999)014<0384:TMCVFF>2.0.CO;2).
46. Senatore, A., Furnari, L., & Mendicino, G. (2020). Impact of high-resolution sea surface temperature representation on the forecast of small Mediterranean catchments' hydrological responses to heavy precipitation. *Hydrology and Earth System Sciences*, **24**(1), 269-291, <https://doi.org/10.5194/hess-24-269-2020>.
47. IDESCAT, Institut d'Estadística de Catalunya (2024). Nombre de municipis i població. Comarques i Aran, In Catalan.
48. Peinó, E., Bech, J., & Udina, M. (2022). Performance assessment of GPM IMERG products at different time resolutions, climatic areas and topographic conditions in Catalonia. *Remote Sensing*, **14**(20), 5085, <https://doi.org/10.3390/rs14205085>.
49. Garcia-Benadí, A., Bech, J., Gonzalez, S., Udina, M., & Codina, B. (2021). A new methodology to characterise the radar bright band using doppler spectral moments from vertically pointing radar observations. *Remote Sensing*, **13**(21), 4323, <https://doi.org/10.3390/rs13214323>
50. Seeley, J. T., & Romps, D. M. (2015). Why does tropical convective available potential energy (CAPE) increase with warming?. *Geophysical Research Letters*, **42**(23), 10-429, <https://doi.org/10.1002/2015GL066199>.
51. Raymond, D. J. (2000). Thermodynamic control of tropical rainfall. *Quarterly Journal of the Royal Meteorological Society*, **126**(564), 889-898, <https://doi.org/10.1002/qj.49712656406>.
52. Colby Jr, F. P. (1984). Convective inhibition as a predictor of convection during AVE-SESAME II. *Monthly Weather Review*, **112**(11), 2239-2252. [https://doi.org/10.1175/1520-0493\(1984\)112%3C2239:CIAAPO%3E2.0.CO;2](https://doi.org/10.1175/1520-0493(1984)112%3C2239:CIAAPO%3E2.0.CO;2)
53. Blanchard, David O. "Assessing the vertical distribution of convective available potential energy." *Weather and forecasting* **13.3** (1998): 870-877. [https://doi.org/10.1175/1520-0434\(1998\)013%3C0870:ATVDOC%3E2.0.CO;2](https://doi.org/10.1175/1520-0434(1998)013%3C0870:ATVDOC%3E2.0.CO;2)
54. del Moral, A., Weckwerth, T. M., Rigo, T., Bell, M. M., & Llasat, M. C. (2020a). C-Band dual-Doppler retrievals in complex terrain: improving the knowledge of severe storm dynamics in Catalonia. *Remote Sensing*, **12**(18), 2930, <https://doi.org/10.3390/rs12182930>.
55. Trapero, L., Bech, J., Rigo, T., Pineda, N., & Forcadell, D. (2009). Uncertainty of precipitation estimates in convective events by the Meteorological Service of Catalonia radar network. *Atmospheric Research*, **93**(1-3), 408-418, <https://doi.org/10.1016/j.atmosres.2009.01.021>.
56. Pineda, N., Peña, J. C., Soler, X., Aran, M., & Pérez-Zanón, N. (2022). Synoptic weather patterns conducive to lightning-ignited wildfires in Catalonia. *Advances in Science and Research*, **19**, 39-49, <https://doi.org/10.5194/asr-19-39-2022>.
57. Schmetz, J., Pili, P., Tjemkes, S., Just, D., Kerkmann, J., Rota, S., & Ratier, A. (2002). An introduction to Meteosat second generation (MSG). *Bulletin of the American Meteorological Society*, **83**(7), 977-992, [https://doi.org/10.1175/1520-0477\(2002\)083<0977:AITMSG>2.3.CO;2](https://doi.org/10.1175/1520-0477(2002)083<0977:AITMSG>2.3.CO;2).
58. van Oldenborgh, Jan, G., Balmaseda, M. A., Ferranti, L., Stockdale, T. N., & Anderson, D. L. (2005). Evaluation of atmospheric fields from the ECMWF seasonal forecasts over a 15-year period. *Journal of Climate*, **18**(16), 3250-3269, <https://doi.org/10.1175/JCLI3421.1>.
59. Bauer, P., Sandu, I., Magnusson, L., Mladek, R., & Fuentes, M. (2020). ECMWF global coupled atmosphere, ocean and sea-ice dataset for the Year of Polar Prediction 2017–2020. *Scientific Data*, **7**(1), 427, <https://doi.org/10.6084/m9.figshare.13013528>.
60. Busquets, E., Udina, M., Bech, J., & Mercader, J. (2025). Sea surface temperature updating impacts on WRF simulations during a heatwave period. *Atmospheric Research*, **108230**, <https://doi.org/10.1016/j.atmosres.2025.108230>.
61. Soula, S., & Chauzy, S. (2001). Some aspects of the correlation between lightning and rain activities in thunderstorms. *Atmospheric research*, **56**(1-4), 355-373, [https://doi.org/10.1016/S0169-8095\(00\)00086-7](https://doi.org/10.1016/S0169-8095(00)00086-7).
62. Pineda, N. & Montanyà, J. (2009). Lightning Detection in Spain: The Particular Case of Catalonia. In: Betz, H.D., Schumann, U., Laroche, P. (eds) *Lightning: Principles, Instruments and Applications*. Springer, Dordrecht, pp. 161–185. https://doi.org/10.1007/978-1-4020-9079-0_7.

63. Sun, J., Chai, J., Leng, L., & Xu, G. (2019). Analysis of lightning and precipitation activities in three severe convective events based on doppler radar and microwave radiometer over the Central China region. *Atmosphere*, *10*(6), 298., <https://doi.org/10.3390/atmos10060298>.
64. Rigo, T., & Farnell, C. (2023). A Summary of Hail Events during the Summer of 2022 in Catalonia: A Comparison with the Period of 2013–2021. *Remote Sensing*, *15*(4), 1012, <https://doi.org/10.3390/rs15041012>.
65. Llasat, M. C., Marcos-Matamoros, R., Pascual, R., Rigo, T., Insúa-Costa, D., & Crespo-Otero, A. (2025). Western Mediterranean flash floods through the Lens of Alcanar (NE Iberian Peninsula): Meteorological drivers and trends. *Atmospheric Research*, 108266, <https://doi.org/10.1016/j.atmosres.2025.108266>.
66. Rigo, T., & Vilar-Bonet, F. (2025). A New Methodology for Detecting Deep Diurnal Convection Initiations in Summer: Application to the Eastern Pyrenees. *Geomatics*, *5*(4), 72, <https://doi.org/10.3390/geomatics5040072>.
67. del Moral, A., del Carmen Llasat, M., & Rigo, T. (2020b). Connecting flash flood events with radar-derived convective storm characteristics on the northwestern Mediterranean coast: Knowing the present for better future scenarios adaptation. *Atmospheric Research*, *238*, 104863, <https://doi.org/10.1016/j.atmosres.2020.104863>.
68. Llasat, M. C., Llasat-Botija, M., Rodriguez, A., and Lindbergh, S., 2010: Flash floods in Catalonia: a recurrent situation, *Adv. Geosci.*, *26*, 105–111, <https://doi.org/10.5194/adgeo-26-105-2010>
69. Llasat, M. C., Marcos, R., Turco, M., Gilabert, J., & Llasat-Botija, M. (2016). Trends in flash flood events versus convective precipitation in the Mediterranean region: The case of Catalonia. *Journal of Hydrology*, *541*, 24–37. <https://doi.org/10.1016/j.jhydrol.2016.05.040>
70. Doswell III, C. A., Brooks, H. E., & Maddox, R. A. (1996). Flash flood forecasting: An ingredients-based methodology. *Weather and forecasting*, *11*(4), 560–581, [https://doi.org/10.1175/1520-0434\(1996\)011<0560:FFFAIB>2.0.CO;2](https://doi.org/10.1175/1520-0434(1996)011<0560:FFFAIB>2.0.CO;2).
71. Thurai, M., Deguchi, E., Iguchi, T.; & Okamoto, K (2003). Freezing height distribution in the tropics. *International journal of Satellite communications and Networking*, *21*(6), 533–545. <https://doi.org/10.1002/sat.768>
72. Farnell, C., Rigo, T., & Heymsfield, A. (2022). Shape of hail and its thermodynamic characteristics related to records in Catalonia. *Atmospheric Research*, *271*, 106098, <https://doi.org/10.1016/j.atmosres.2022.106098>.
73. Wu, P., Hara, M., Hamada, J. I., Yamanaka, M. D., & Kimura, F. (2009). Why a large amount of rain falls over the sea in the vicinity of western Sumatra Island during nighttime. *Journal of Applied Meteorology and Climatology*, *48*(7), 1345–1361, <https://doi.org/10.1175/2009JAMC2052.1>.
74. Caracena, F., Maddox, R. A., Hoxit, L. R., & Chappell, C. F. (1979). Mesoanalysis of the Big Thompson storm. *Monthly Weather Review*, *107*(1), 1–17, [https://doi.org/10.1175/1520-0493\(1979\)107<0001:MOTBTS>2.0.CO;2](https://doi.org/10.1175/1520-0493(1979)107<0001:MOTBTS>2.0.CO;2).
75. Vitale, J. D., & Ryan, T. (2013). Operational Recognition of High Precipitation Efficiency and Low-Echo-Centroid Convection. *Journal of Operational Meteorology*, *1*(12), 128–143, <http://dx.doi.org/10.15191/nwajom.2013.0112>.

Disclaimer/Publisher's Note: The statements, opinions and data contained in all publications are solely those of the individual author(s) and contributor(s) and not of MDPI and/or the editor(s). MDPI and/or the editor(s) disclaim responsibility for any injury to people or property resulting from any ideas, methods, instructions or products referred to in the content.